THE BEHAVIOUR OF LITHIUM AND SODIUM IRON OXIDES AS CATHODE MATERIALS FOR LITHIUM BATTERIES

by

Monique Richard

B.Sc., University of New Brunswick, Fredericton, 1994

A Thesis Submitted in Partial Fulfillment of the Requirements for the

Degree of Master of Science

in the Department

of

Physics

© Monique Richard 1996

Simon Fraser University

June 1996

All rights reserved. This thesis may not be reproduced, in whole or in part, by photocopy or other means, without permission of the author.

APPROVAL

Name:	Monique Richard
Degree:	Master of Science
Title of Thesis:	The Behaviour of Lithium and Sodium Iron Oxides as Cathode Materials for Lithium Batteries.

Examination Committee:

Chair: Dr. Simon Watkins

Dr. Jeff Dahn
Senior Supervisor

Dr. Bob Frindt

Dr. Daniel Loss

Dr. Albert Curzon
Internal Examiner

Date Approved: June 21, 1996

PARTIAL COPYRIGHT LICENSE

I hereby grant to Simon Fraser University the right to lend my thesis, project or extended essay (the title of which is shown below) to users of the Simon Fraser University Library, and to make partial or single copies only for such users or in response to a request from the library of any other university, or other educational institution, on its own behalf or for one of its users. I further agree that permission for multiple copying of this work for scholarly purposes may be granted by me or the Dean of Graduate Studies. It is understood that copying or publication of this work for financial gain shall not be allowed without my written permission.

Title of Thesis/Project/Extended Essay

The Behaviour of Lithium and Sodium Iron Oxides as Cathode Materials for Lithium Batteries.

Author.
(signature)

Monique Richard
(name)

25 June 1996
(date)

ABSTRACT

Lithium transition metal oxide cathodes are the state of the art cathode materials used in lithium batteries. The most promising of these materials, in terms of availability of materials, cost and safety, are $LiNiO_2$, $LiCoO_2$, $LiMnO_2$, $LiMn_2O_4$ and $LiFeO_2$. The electrochemical behaviour of the first four of these materials has been and is being thoroughly studied. However, evidence of similar studies on $LiFeO_2$ is not available in part because a layered phase of $LiFeO_2$ has only recently been discovered.

In 1987, Nalbandyan and Shukaev reported the first synthesis of a layered phase of $LiFeO_2$ which is isostructural to $LiNiO_2$ and $LiCoO_2$. The latter two materials have been shown to perform well in rechargeable lithium batteries. This similarity to $LiNiO_2$ and $LiCoO_2$ prompted us to undertake a study of layered $LiFeO_2$.

We synthesized the layered phase of $NaFeO_2$, the precursor needed to form layered $LiFeO_2$. As expected, $NaFeO_2$ is very sensitive to preparation conditions but a successful synthesis was achieved. The layered $LiFeO_2$ phase was formed via an ion exchange reaction between the layered $NaFeO_2$ material and $LiNO_3$ at 300°C.

The electrochemical behaviour of the $LiFeO_2$ material was examined by constructing cells and cycling these at constant current. The results suggested that very little lithium could be removed from the structure. We also studied the electrochemical behaviour of $NaFeO_2$ versus lithium metal. The study was attempted in order to determine if sodium atoms could be removed on charge and if lithium atoms could, on the subsequent discharge, be electrochemically substituted into the iron oxide lattice. The results suggest that this can occur to some extent.

In-situ x-ray cells were used in order to determine what happened to the structure of the iron oxide materials as lithium/sodium was removed. However, a first attempt with a traditional in-situ cell design yielded poor data which suffered from low signal to background. As a result, a new in-situ cell was developed.

This new cell uses 'plastic' electrodes which give a 5-fold increase in signal to background. The plastic technology was first tested on a known material, $LiMn_2O_4$, to verify that it worked well.

Then the plastic technology was used on $LiFeO_2$ and $NaFeO_2$. The results for $LiFeO_2$ confirmed that no lithium could be withdrawn from the structure prior to the onset of electrolyte decomposition. Thus, $LiFeO_2$ is not a cathode material of interest for rechargeable lithium batteries.

ACKNOWLEDGMENTS

There are many people without whose support and encouragement I wouldn't be enrolled in this program and wouldn't be this close to completion.

First, thanks to my mother and brothers, Luc and Michel. They may not have always understood what I was doing, or its ultimate purpose, but they were always interested and supportive.

To my friends and classmates, both from UNB and from SFU. Through their commiserations they made classes and the problems associated with research more bearable.

Thanks to Ian and Alf who proof read this thesis, with no gain to themselves, as a favor to me.

Finally, thanks to Dr. Jeff Dahn. In the two years I've been a graduate student at SFU, you taught me a lot about science and research and you guided me through the research presented here.

Thanks to all of you.

Table of Contents

LIST OF FIGURES

LIST OF TABLES

CHAPTER ONE

1. INTRODUCTION

There are many rechargeable battery technologies available today. They range from lead-acid to lithium ion and the choice of which to use depends on the sort of work to be done by the battery. The most promising rechargeable batteries are nickel metal hydride (NiMH), nickel cadmium (NiCad) and lithium-ion cells (Way, 1995).

NiMH batteries outperform NiCad's and are used in consumer electronics. NiMH cells have high volumetric energy density (energy per unit volume) but large mass density and therefore relatively low specific gravimetric energy density (energy per unit mass). Lithium-ion batteries are state-of-the-art because they have high energy densities, high voltages, good cycling ability and long life compared to NiMH (Way, 1995). Lithium-ion batteries are useful for certain applications but improvements need to be made in order to keep pace with the miniaturization of consumer electronics. In particular the size and weight of the batteries must be reduced while the amount of energy stored is maintained. These are determined, in part, by the capacities of the electrode materials used. For lithium batteries, capacity loosely refers to the amount of lithium that can be removed and inserted into the electrode material. The greater the specific capacity of the material, the more charge can be stored by a certain mass of material. Therefore, research continues in order to develop materials with the highest specific capacities possible in order to store the most charge in the least mass. The result would be a battery with higher energy density.

Beyond the demands of the electronics market there also exists the demand for better batteries for use in electric vehicles (EV). The latter demand has evolved as a result of legislation enacted in California which will force manufacturers to sell a percentage of emission free vehicles such as EV's.

1.1 Lithium Batteries with Lithium Metal Anodes

Lithium batteries normally rely on the intercalation of lithium into host solids as the reaction mechanism. Intercalation is the process which allows atoms to be reversibly inserted into the lattice of a host material. The main feature of intercalation is that the insertion does not cause any significant structural change to the host lattice, but merely a slight expansion. In the 1970's, scientists realized that the reversibility of the intercalation process could be exploited to make rechargeable batteries (Dahn and McKinnon, 1988). However, not all structures allow the insertion and removal of an atom in this fashion, so researchers needed to develop appropriate host materials. The study of such materials has been ongoing. The result has been the development of a technology for lithium batteries involving a transition metal oxide (TMO) cathode and a lithium metal anode. An example of a cell now in commercial production is the Li/MnO_2 camera battery (non-rechargeable) produced by Duracell and others. This cell could be designed to be rechargeable but for safety reasons has not been.

The process of cell cycling is described in Figures 1-1(A) and 1-1(B). Figure 1-1(A) describes the discharge process. The lithium in the lithium metal anode has a higher chemical potential and so is less tightly bound than it would be in the TMO. In

other words, the free energy of a lithium atom is lower in the intercalation host than in the lithium metal. As a result, the cell is in a position to do electrical work. Lithium atoms are stripped from the lithium electrode and separate into an electron and a lithium ion. The lithium ions dissolve into the electrolyte and the associated electrons travel to the cathode, via the external circuit, doing work in the process. The ion and electron recombine at the surface of the TMO, and then diffuse from the surface of the TMO to the bulk (Dahn and McKinnon, 1988). In many TMO's, the lithium spends most of its time localized on specific sites of the lattice. The TMO host then has two roles:

(1) to provide a lattice of sites where the guest lithium atoms may reside; and

(2) to determine the interactions between the guest atoms. These interactions are complicated since they are composed of Coulomb interactions, screened by the electrons in the host, and elastic interactions caused by the distortion of sites by the guest atoms.

Figure 1-1(B) describes the charging process. The cell is charged using a constant current. Work must be done in order to remove lithium from the TMO since lithium has a lower chemical potential in the TMO than it does in lithium metal. At this point the lithium ions are forced out of the cathode and into the electrolyte solution. The electrons travel, via the external circuit, to the anode. The lithium ions travel through the electrolyte solution into the anode. As more lithium is removed, the remaining lithium becomes more tightly bound, resulting in an increase in the voltage necessary to remove more lithium. The lithium ion and the electron recombine at the lithium metal anode.

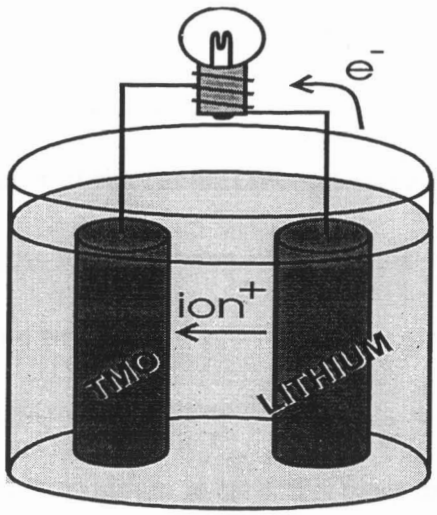

Figure 1-1(A): Schematic diagram describing the discharge process for a lithium secondary cell

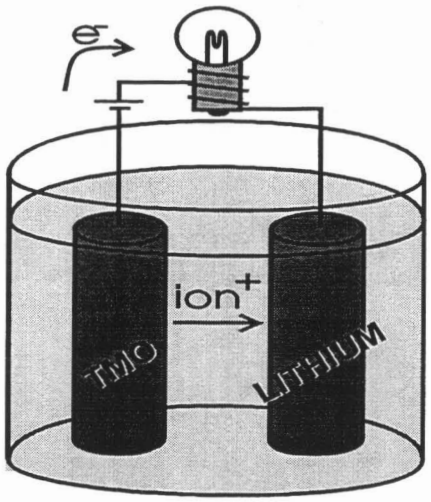

Figure 1-1(B): Schematic diagram describing the charging process in a lithium secondary cell.

Theoretically the secondary cell described above should function perfectly, however early attempts to implement the technology showed it had some safety flaws due to the presence of the lithium metal anode (Dahn et al., 1991).

1.2 Lithium Ion Cells

Because of the safety problems encountered with the use of lithium metal, it is necessary to change the concept of the lithium secondary cell and somehow remove the lithium metal. One approach is to replace the lithium metal with a carbon anode. The reason carbons were chosen are twofold:

1) they can reversibly intercalate lithium; and

2) the chemical potential of lithium in carbon is close to that of lithium in lithium metal (see Figure 1-2), so the voltage of a cell is maintained.

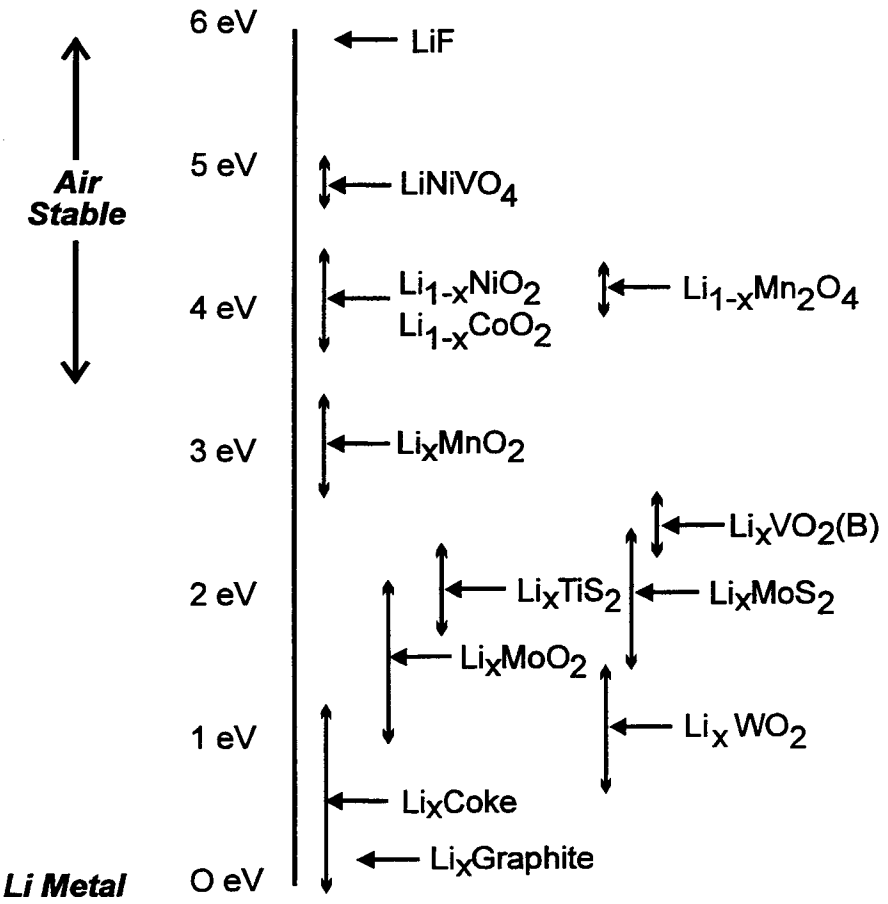

Figure 1-2: Binding energy chart for different lithium transition metal compounds. Voltages are defined versus lithium metal as in equation (1-1) (Way, 1995).

A battery with a lithium transition metal oxide cathode and a carbon anode is called a lithium-ion cell, or a rocking chair cell. The latter name is used because the lithium "rocks" back and forth between the two electrodes during cell operation. In such a cell all the lithium to be used in the cycling process is contained in the cathode and so the cell must be charged prior to use. Lithium enters the carbon via the intercalation process, much like it enters the cathode. The result is a slight expansion between the graphite layers.

The operation of a lithium ion cell is independent of the type of lithium transition metal oxide used. The type of transition metal oxide determines the details of the electrochemical behaviour of the cell, but its basic operating principles are unaffected. Figure 1-3 illustrates the charge cycle of a lithium-ion cell. The anode is carbon and the cathode is $LiMO_2$ (M = Ni, Co, Mn, Fe). During discharge, as mentioned above, lithium is returned to the cathode as it is simultaneously being removed from the carbon anode.

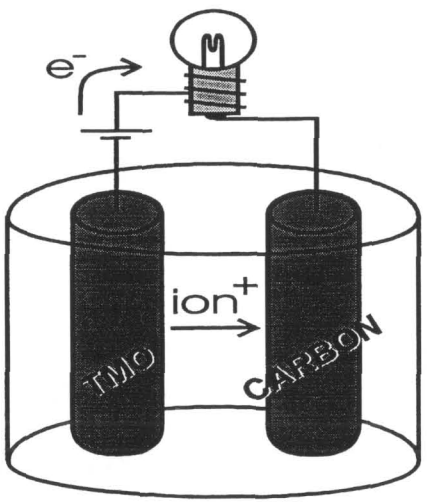

Figure 1-3: Schematic diagram describing the charge process in a lithium-ion (rocking chair) cell

Assuming that some amount, x, of lithium was originally removed from the cathode, then the composition of the cathode at the end of the charge part of the cycle is $Li_{1-x}MO_2$. Some lithium originally in the cathode is lost during the first charge due to the formation of a passivation film on the carbon (Dahn et al., 1991). The amount of lithium that enters the carbon is y, where $y<x$, which corresponds to an anode having a chemical composition of Li_yC_6. The amount of lithium lost is proportional to the surface area of the carbon (Dahn et al., 1991). Upon discharge, all of the lithium that was intercalated into the carbon on charge is returned to the cathode. The half cell reactions found to be occurring for the particular case of the lithium transition metal oxide versus carbon cell, can then be written as:

$$LiMO_2 \rightarrow Li_{1-x}MO_2 + xLi^+ + xe^- \qquad \text{(first charge)}$$

$$C_6 + xLi^+ + ye^- + \text{electrolyte} \rightarrow Li_yC_6 + Li_{x-y}\text{electrolyte} \qquad \text{(first charge)}$$

where Li_{x-y} electrolyte represents the reaction product between lithium and the electrolyte. No further lithium is lost on subsequent cycling, so the reactions may be written as:

$$Li_yC_6 \rightarrow C_6 + yLi^+ + ye^- \qquad \text{(discharge process)}$$

$$Li_{1-x}MO_2 + yLi^+ + ye^- \rightarrow Li_{1-x+y}MO_2 \qquad \text{(discharge process)}$$

and

$$Li_{1-x+y}MO_2 \rightarrow Li_{1-x}MO_2 + yLi^+ + ye^- \qquad \text{(subsequent charge)}$$

$$C_6 + yLi^+ + ye^- \rightarrow Li_yC_6 \qquad \text{(subsequent charge)}$$

This technology displays a lower energy density compared to cells containing lithium metal, however this loss is more than compensated by increased safety and longer

cycle life. Research continues since improvements concerning energy density, cost and safety are still needed to make these batteries applicable in EV's. It is to this latter end that materials research is important in order to study new materials and so determine which are economically and scientifically viable.

The materials are chosen such that the chemical potentials of lithium atoms in both electrodes are as widely different as possible. This choice of materials results in a high voltage since the voltage of the cell is given by :

$$V = \frac{-(\mu_{cath} - \mu_{anode})}{e} \qquad (1\text{-}1)$$

In equation (1-1), μ_{cath} is the chemical potential of the lithium in the cathode and μ_{anode} is the chemical potential of lithium in the anode. If the anode is lithium metal, then $\mu_{anode} = \mu_{Li}$

Figure 1-2 , from (Way, 1995), shows some of the materials that have been studied as electrode materials for lithium batteries. From Figure 1-2, the cathode has a high voltage versus lithium metal and the anode, a low voltage versus lithium metal. Figure 1-2 indicates that the most desirable cathode materials are lithium transition metal oxides since they have voltages between 3 and 5 volts versus lithium metal. This voltage range is desired in order to make these batteries useful in consumer electronics and to make them compatible with existing electrolytes. In order to be of use in a battery, the lithium transition metal oxide must be stable in air, thereby making synthesis of the material practical. It must be able to hold a large amount of lithium that can be reversibly deintercalated and it must have a large voltage versus lithium metal. These

considerations reduce the list of transition metal oxides that can be used to those containing Mn, Co, Ni, Cr, V, Ti and Fe. Iron compounds are not listed in Figure 1-2 because they have not been carefully studied. However, they might demonstrate the qualities above since they can be synthesized in the same structure as $LiNiO_2$ or $LiCoO_2$.

There are presently batteries on the market that contain either $LiNiO_2$ or $LiCoO_2$. These have demonstrated good cycling ability, reasonably long shelf lives, of a two to three years, and the ability to be recharged hundreds of times. These would seem to be good materials were it not for the high cost of the raw materials, the difficulties in obtaining materials that are single phase and the fact that these materials are slightly toxic.

Referring then to Figure 1-2 and taking the above factors into account, the best choices for a cathode material would seem to be $LiMnO_2$ and $LiMn_2O_4$. We could also potentially include some type of lithium iron oxide in this list although its usefulness as a cathode material needs to be verified.

The subject of this thesis is the $NaFeO_2$ and $LiFeO_2$ system. These materials could theoretically be the best possible material, since the cost of iron is low and the theoretical capacity for the removal of all the lithium is high. Studies of the behavior of the iron oxide materials, when cycled versus lithium, have not been performed in part because of the difficulty in the production of the layered lithium iron oxide phase. Furthermore, materials of the form $LiFe_xNi_{1-x}O_2$ have demonstrated that the addition of iron to the material drastically reduces the reversible capacity (Reimers et al., 1993).

For $NaFeO_2$, electrochemical methods were used to attempt to substitute lithium atoms for sodium atoms in the iron oxide structure. The sodium atoms might be removed during the first charge. The lithium from the electrolyte would be inserted into the iron oxide lattice during the next discharge since the concentration of lithium atoms in the electrolyte is greater than that of sodium atoms after a full charge. The cycling process is very similar to that described previously except that after the first charge the electrolyte might contain a significant portion of sodium atoms.

Optimistically, the half cell reactions might proceed in the following fashion:

$$NaFeO_2 \text{ --> } Na_{1-x}FeO_2 + x\,Na^+ + x\,e^- \qquad \text{(first charge)}$$

$$Na_{1-x}FeO_2 + yLi^+ + ye^- \text{ --> } Na_{1-x}Li_yFeO_2 \qquad \text{(first discharge)}$$

$$Na_{1-x}Li_yFeO_2 \text{ --> } Na_{1-x}FeO_2 + y\,Li^+ + y\,e^- \qquad \text{(subsequent recharge)}$$

These half cell reactions were studied via electrochemical measurements performed versus lithium metal. Lithium metal was used because of the need to study the behaviour of the cathode with respect to a reference electrode. Since the behaviour of many cathodes versus lithium metal is well known, it is the logical choice.

The first step in the study was to make the α-phase of sodium iron oxide. It is thermodynamically unstable during synthesis and tends to preferentially form the beta or gamma-$NaFeO_2$ phases if the heating proceeds for too long. Layered lithium iron oxide is obtained via an ion exchange reaction involving alpha-$NaFeO_2$ and $LiNO_3$. Materials synthesis will be discussed in detail in chapter two.

Lithium iron oxide exists in four different phases, alpha (disordered rock salt), beta (monoclinic), gamma (tetragonal) and hexagonal/layered. Of these, the hexagonal

phase is the most promising. Its structure and that of the other phases will be discussed in chapter 3.

Because layered $NaFeO_2$ is unstable during synthesis, it is necessary to check to make sure the desired alpha structure is obtained. Powder x-ray diffraction is used to determine the structure of the sample. The x-ray diffraction method and the results obtained will be discussed in chapter 4. The Rietveld refinement method was used to generate a theoretical fit to the experimental pattern. The results were used to confirm the existence of the desired phase. Similar studies on $LiFeO_2$ were also performed. The Rietveld method and its results will also be discussed in chapter 4.

Electrochemical studies of the layered $LiFeO_2$ and $NaFeO_2$ materials were made next. Experimental details of cell construction and cycling are discussed in chapter 5. The iron oxide materials were also studied in an in-situ x-ray cell. Such a cell is equipped with a beryllium x-ray window so that crystallographic changes, if any, in the electrode material can be studied in-situ while the cell is charged or discharged. To improve signal to noise of the data a new Bellcore plastic electrode technology (Gozdz ,1994, Amatucci, 1995) was adopted. These studies entailed the development of the Bellcore plastic electrode technology. The development of this plastic technology and the ensuing results from the in-situ electrochemical studies will be discussed in chapter 6.

The results of all these different studies will be summarized in chapter 7 and suggestions will be made for further work based on the conclusions drawn from this work.

CHAPTER TWO

2. EXPERIMENTAL - PART I

The synthesis of $LiFeO_2$ is a two step process . The first step is the production of alpha-$NaFeO_2$. Having successfully synthesized the sodium iron oxide compound, an ion exchange reaction is used to replace the sodium atoms in the material with lithium atoms. This chapter will discuss both steps in the process. The synthesis process is time consuming and attempts were made to find alternate routes to $LiFeO_2$ by using other familiar synthesis procedures: spray dryer, different salts for the ion exchange and an aqueous method. These will also be discussed.

2.1 Synthesis of $NaFeO_2$

The synthesis of $LiFeO_2$ is a two step process as suggested in the literature (Nalbandyan and Shukaev, 1987). The first step is the production of $NaFeO_2$, by mixing $Na_2C_2O_4$ with alpha-Fe_2O_3 followed by heating. The reaction is:

$$Na_2C_2O_4 + Fe_2O_3 \rightarrow 2\,NaFeO_2 + 2CO + 1/2\,O_2\,. \qquad (2\text{-}1)$$

The reactant powders were ground together for 15 minutes. The powder mixture was then loosely packed into an alumina boat and fired at 600°C in air for 20 hours. Nalbandyan and Shukaev (1987) suggest following this first heating with regrinding, compression of the material into a pellet and reheating for a further 20 hours at 650°C. This step was found to be unnecessary here. Other researchers (Hewston and Chamberland, 1987, Takeda et al., 1980) determined that the synthesis temperature must

be monitored closely since exposure to temperatures in excess of 600^0C causes the beta phase to form. The appearance of the beta phase of $NaFeO_2$ was observed when alternate synthesis routes were examined.

2.2 Synthesis of $LiFeO_2$ By Ion Exchange

The second step in the synthesis process involves an ion exchange reaction. An ion exchange reaction is the reversible interchange of ions between the solid phase, $NaFeO_2$, and a liquid phase, $LiNO_3$, at 300°C. By definition, an ion exchange maintains the electroneutrality of both the solid and the liquid phases at all time. As a result, the ion exchange proceeds in equal amounts in both directions. The process proceeds as described in equation 2-2.

$$NaFeO_2 + 10\ LiNO_3 \text{ --> } LiFeO_2 + NaNO_3 + 9LiNO_3 \qquad (2\text{-}2)$$

The mixture of the two solids proceeded in an alumina crucible at 300°C for 18 hours. The $NaFeO_2$ was pressed into pellets at 2000psi and completely surrounded in loosely packed $LiNO_3$ salt. The pellets typically weighed two to three grams, so in general more than one pellet was used. This synthesis temperature is necessary in order to melt the lithium nitrate, which according to (Merck, 1989) has a melting point of 270°C. This temperature also had the advantage of being far from the temperature for the alpha to beta $NaFeO_2$ transition so the chances of causing a phase transition in the iron oxide material are minimized.

This second process is slightly different from that used by Nalbandyan and Shukaev (1987) which suggests using a fifty fold excess of lithium nitrate in order to ensure that only lithium will remain in the compound. Instead, the process described by equation (2-2) uses a ten fold excess of lithium nitrate and was found to produce a satisfactory lithium iron oxide end product.

Following the 18 hour exchange time, the melt produced by the excess lithium nitrate and the sodium nitrate, was poured out of the crucible into a nickel foil boat. The remaining $LiFeO_2$ powder was quickly treated with ethanol as suggested (Nalbandyan and Shukaev, 1987) in order to prevent the powder from reacting with water vapour. The resulting solid, which is wet, was ground in order to obtain reasonably small particle size. This mixture is mixed with ethanol and placed in an ultrasonic bath for 30 minutes in order to remove any remaining lithium nitrate which according to (Merck, 1989) dissolves in the alcohol. The solution is filtered through filter paper and the resulting powder dried in an oven at 120°C for an hour. The powder is then studied by x-ray diffraction in order to ensure that $LiFeO_2$ is produced.

The total synthesis time for $LiFeO_2$ is 38 hours. This is the most time consuming part of the study so attempts were made to find alternate synthesis routes which would yield the same quality alpha-$LiFeO_2$ in a shorter period of time. These attempts included:

(1) aqueous ion exchange between 4M LiOH and $NaFeO_2$ at 90°C for 20 hours.

(2) direct mixing of $LiOH \bullet H_2O$ and Fe_2O_3 to produce $LiFeO_2$

(3) spray dryer method for mixing 1M $LiNO_3$ and $Fe(NO_3)_3.9H_2O$. The method produces a very well mixed powder containing Li, Fe, O, N and other atoms. These mixtures were heated at 630°C for 90 hours.

None of these methods proved successful in producing $LiFeO_2$. Instead the reactants were completely unreacted for the aqueous ion exchange or they produced alternate phases for the other two methods.

2.3 Synthesis of $NaFe_{(1-x)}Co_xO_2$

Because $NaFeO_2$ is so sensitive to the synthesis temperature, attempts were made to stabilize the material by substituting cobalt atoms for iron. It was believed that cobalt would stabilize the structure because $LiCoO_2$ can be readily made in the layered structure and is stable. The intention was to make the structure more stable so that when sodium or lithium, in the associated lithium iron cobalt oxide material, is removed the structure remains intact.

The synthesis process for the cobalt doped materials proceeded in the following fashion.

$$Na_2C_2O_4 + x\ Fe_2O_3 + (1\text{-}x)\ CoO \rightarrow 2\ NaFe_xCo_{(1-x)/2}O_2 + 2CO + \frac{(2x-1)}{2} O_2 \qquad (2\text{-}3)$$

The powders were ground together for 15 minutes then loosely packed into an alumina boat. The synthesis proceeded at 600°C for 20 hours for x = 0.1.

The composition of the resulting powder was determined by x-ray diffraction. The pattern showed peaks of a phase of the same structure as $NaFeO_2$, suggesting that the Co atoms were substituted for iron as desired. It was then submitted to the same ion exchange process as described above.

Similar types of synthesis approaches were attempted with nickel and chromium. Those reactions proceeded according to equations 2-4 and 2-5.

$$Na_2C_2O_4 + x\ Fe_2O_3 + (1\text{-}x)/2\ Cr_2O_3 \rightarrow 2\ NaFe_xCr_{(1-x)/2}O_2 + 2CO + \frac{(3x-1)}{4}O_2 \qquad (2\text{-}4)$$

$$Na_2C_2O_4 + x\ Fe_2O_3 + (1\text{-}x)\ NiO \rightarrow 2\ NaFe_xNi_{(1-x)/2}O_2 + 2CO + \frac{(2x-1)}{2}O_2 \qquad (2\text{-}5)$$

As described above, these reactions proceeded in alumina boats for 20 hours at 600°C for x=0.1. X-ray diffraction studies on the end products of these reactions showed that $NaFeO_2$ was produced but the NiO was incompletely reacted. The chromium doped samples showed $NaFeO_2$ peaks and some unidentified peaks. Thus, the reactions in equations 2-4 and 2-5 did not occur as planned.

CHAPTER THREE

3. INTERCALATION IN $NaFeO_2$ AND $LiFeO_2$

Intercalation is the reversible insertion of a guest atom into a host lattice. By definition, the insertion or removal of the guest does not change the lattice significantly but can cause a slight expansion or contraction. This process may proceed in a variety of ways which are determined by the lattice structure of the host material. In the case of a layered material such as $LiFeO_2$, the lithium forms sheets between two oxygen layers.

The intercalation process is more favourable in certain lattice types than in others. This is the situation in the lithium iron oxide materials. Although lithium iron oxide exists in four phases, only one of these is thought to be favourable for use as an intercalation host. The differences between the structures of the four phases will be discussed in this chapter as well as the process of intercalation in layered materials.

3.1 Structure of $NaFeO_2$ and $LiFeO_2$

Lithium iron oxide exists in four phases, alpha (cubic), beta (monoclinic or tetragonal), gamma (tetragonal) and layered (hexagonal) . The lattice parameters for the different phases are given in Table 1.

Table 1: The lattice parameters for the four phases of $LiFeO_2$ and for layered $NaFeO_2$.

phase of material	crystal system	space group	a	b	c	β
alpha-$LiFeO_2$	cubic	Fm3m	4.158	4.158	4.158	-
beta-$LiFeO_2$ (1)	tetragonal	I4/m	2.89	2.89	4.28	-
beta -$LiFeO_2$ (2)	monoclinic	C2/c	8.571	11.59	5.147	145.70°
gamma-$LiFeO_2$	tetragonal	I4/m	4.05	4.05	8.74	-
layered-$LiFeO_2$	hexagonal	R-3m	2.956	2.956	14.57	-
alpha-$NaFeO_2$	hexagonal	R-3m	3.024	3.024	16.07	-

(1) parameters obtained from (Anderson and Schieber, 1964)
(2) parameters obtained from (Famery et al., 1985, Hewston and Chamberland, 1987)

According to Cox et al. (1963), the alpha phase of $LiFeO_2$ was first reported by Posnjak et al. in 1933 as an early example of a compound exhibiting random cation mixing on the same lattice sites. It has a disordered cubic NaCl type structure (Hewston and Chamberland, 1987) which is given schematically in Figure 3-1 (Cox et al., 1963). The lattice parameters for the structure are given in Table 1. The smaller half shaded circles indicate that the position in the lattice may be occupied by either a lithium or an iron atom. This random assignment of the cations to the lattice sites prevents the possibility of using this structure as an intercalation compound since it would be impossible to remove any significant amount of lithium without the interference of neighbouring oxygen and iron atoms.

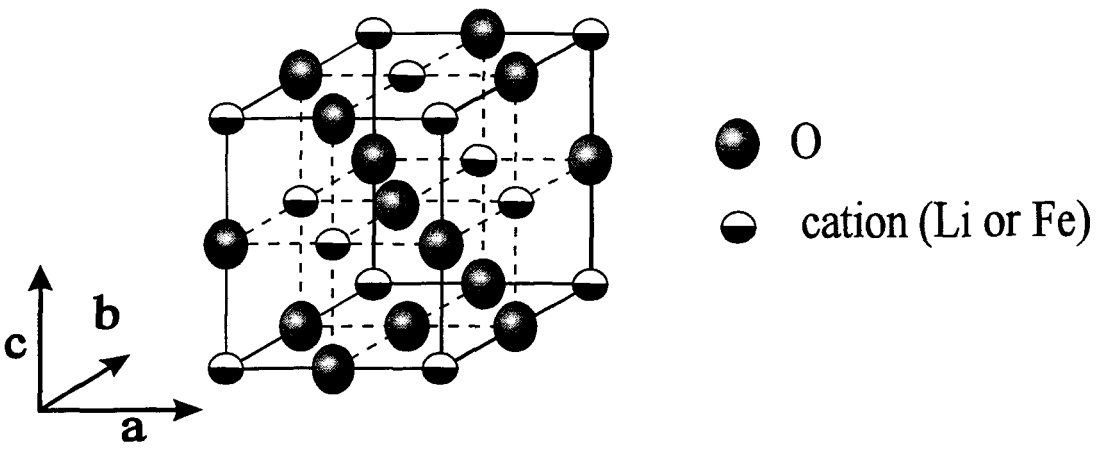

Figure 3-1: Alpha phase of lithium iron oxide, $LiFeO_2$

The beta phase of $LiFeO_2$ is thought to be an unstable intermediate phase that exists between the alpha and gamma phases (Anderson and Schieber, 1964, Cox et al., 1963, Hewston and Chamberland, 1987). Early studies (Anderson and Schieber, 1964, Hewston and Chamberland, 1987) suggested that it had a tetragonal structure, as shown

in Figure 3-2 (Cox et al., 1963), however more recent experiments, using electron microscopy techniques, suggest that it could have a monoclinic structure (Hewston and Chamberland, 1987). The debate concerning the exact nature of the structure of the beta phase has yet to be resolved, so the lattice parameters for both cases are given in Table 1. In the case of the tetragonal structure, Cox et al. (1963) describe it as consisting of alternating layers of lithium and iron atoms in the c direction. The middle layer of the unit cell has lithium atoms surrounded by oxygen nearest neighbours. This layer also has rows of lithium atoms. These rows might allow the lithium to be removed from the material. However the uncertainty concerning the structure of the beta phase has prevented this study.

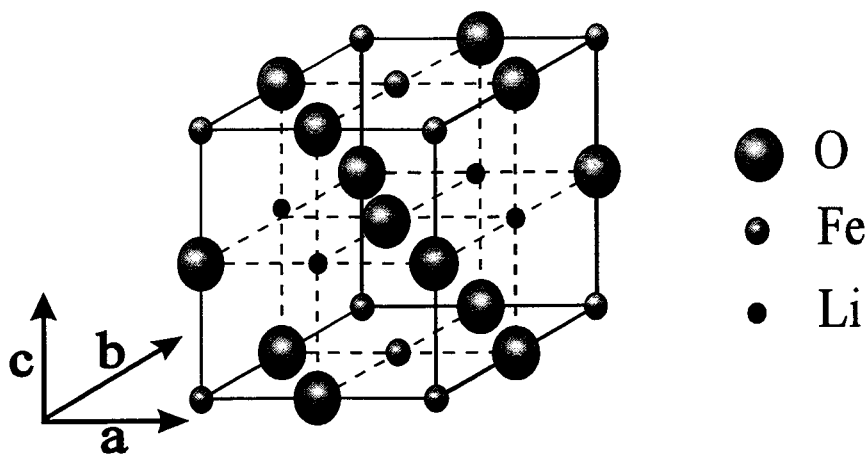

Figure 3-2: Beta phase(1) of lithium iron oxide, $LiFeO_2$

The gamma phase of $LiFeO_2$ is a high temperature phase. According to (Anderson and Chamberland, 1964, Brunel and de Bergevin, 1969, Famery et al., 1985, Hewston and Chamberland, 1987, Nalbandyan and Shukaev, 1987) it has the tetragonal structure shown in Figure 3-3. The lattice parameters for the structure are given in Table

1. The position of the iron atoms on the lattice would probably prevent the removal of lithium through the process of intercalation.

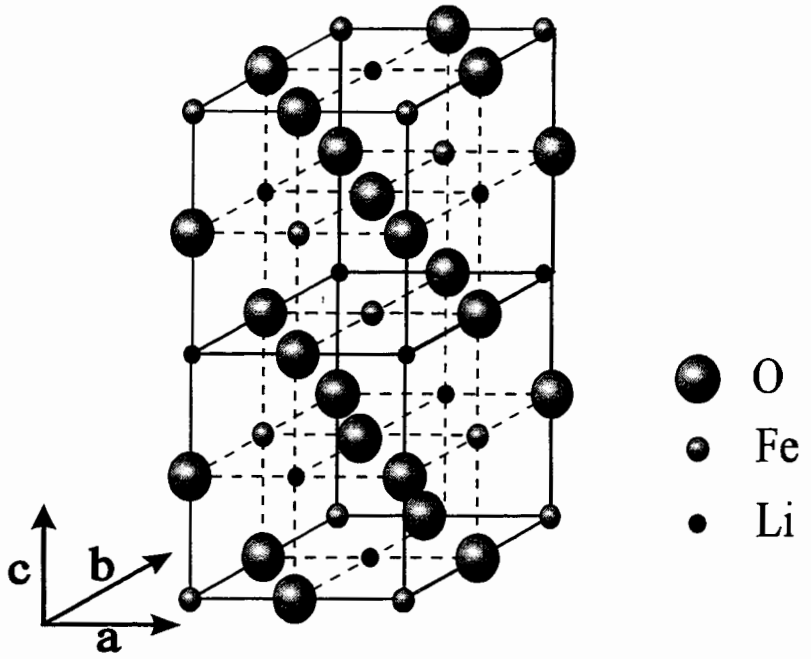

Figure 3-3: Gamma phase of lithium iron oxide, $LiFeO_2$

In 1987, Nalbandyan and Shukaev (1987) reported the synthesis of a fourth phase of $LiFeO_2$. This new phase was based on the known alpha $NaFeO_2$ layered phase, shown in Figure 3-4A, which is isostructural to $LiNiO_2$ and $LiCoO_2$. The latter two materials are known to reversibly intercalate lithium. The synthesis method, which is described in chapter two, involves the formation of the layered $NaFeO_2$ material and then an ion exchange reaction to obtain the layered $LiFeO_2$. This layered phase is shown in Figure 3-4A (Hewston and Chamberland, 1987). This figure describes alpha-$NaFeO_2$ and layered-$LiFeO_2$, the difference between the two being an increase in the spacing along the body diagonal for $NaFeO_2$ since sodium atoms are larger.

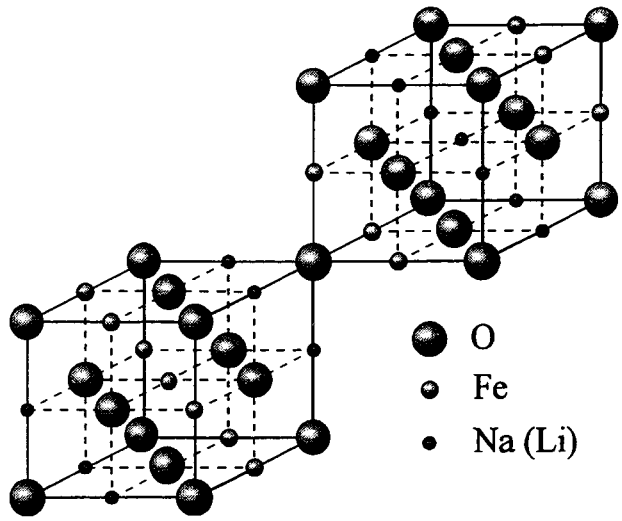

Figure 3-4A: Structure of the layered sodium(lithium) iron oxide

Clearly there are layers of the same type of atoms along the body diagonal of the cube. As a result, the structure can be redrawn as a hexagonal structure as in Figure 3-4B (Hewston and Chamberland, 1987).

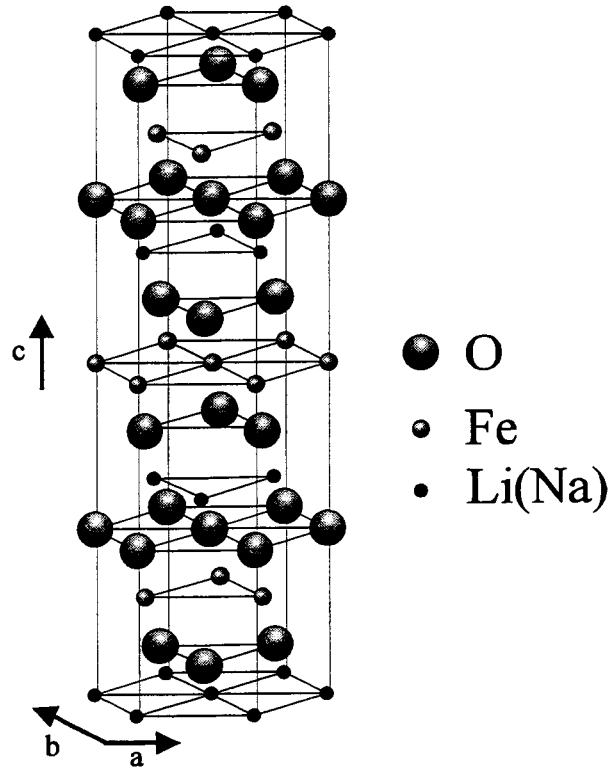

Figure 3-4B: Hexagonal representation of the layered sodium(lithium) iron oxide.

It was mentioned in chapter two that attempts were made to dope the $NaFeO_2$ material with cobalt, nickel or chromium in an attempt to stabilize the structure. These doped $NaFeO_2$ materials would then go through an ion exchange to obtain the doped $LiFeO_2$. These attempts were made under the assumption that the dopant atoms would replace the iron atoms in the lattice. A successful synthesis would then result in materials of the same structure as Figures 3.4A&B. The lattice constants would be slightly different due to the different sized atoms.

3.2 INTERCALATION IN IRON OXIDES

Intercalation is the reversible insertion of guest atoms into a host lattice. For the iron oxide materials studied here, the guest is the lithium or sodium atoms. Figure 3-4B shows clearly that the lithium atoms in this $LiFeO_2$ phase fully occupy layers, as opposed to the alpha, beta and gamma structures where lithium atoms share layers with iron and oxygen atoms. The result of this full layer occupation is the possibility of removing the atoms from these layers.

The removal of lithium from the layered structure of $LiNiO_2$ and $LiCoO_2$ has been shown to be reversible and the purpose of this study is to see if a similar process would occur in $LiFeO_2$. The reversibility of the process would be examined on the subsequent discharge of the cell. Since lithium has a lower chemical potential in the iron oxide, it prefers to return to the iron oxide lattice. Assuming that the initial removal of the lithium atoms was due to de-intercalation, so that the structure was not dramatically changed,

then it should be possible to reinsert the lithium between the adjacent oxygen layers, thereby regaining the original unit cell.

The iron oxide materials were also studied to determine the feasibility of removing sodium atoms from the structure. The removal of the sodium atoms, by intercalation, would be expected to cause changes in the lattice constants. Assuming that intercalation was the process responsible for the removal of the sodium, it could be possible to re-insert lithium, from the electrolyte, into the lattice and so electrochemically replace the sodium atoms with lithium atoms.

CHAPTER FOUR

4. EXPERIMENTAL - PART II: CHARACTERIZATION OF MATERIALS

4.1 X-Ray Diffraction

The synthesis process for $NaFeO_2$ and $LiFeO_2$ described in chapter 2 was followed and orange powders were produced. X-ray diffraction techniques were used in order to verify that the correct phase of the materials had been produced and that they did not contain impurities.

4.1.1 Powder Diffraction

Two diffractometers were used to make powder x-ray diffraction measurements. The first, a Siemens D5000 $\theta - \theta$ diffractometer, operated in the flat plate sample geometry and had a copper target x-ray tube. In the $\theta - \theta$ geometry, the sample is kept fixed and the tube and detector are stepped at 0.05 degrees per 12 seconds in opposite directions to obtain a final angle of 2θ. The divergence slit was set at 0.5°, the antiscatter slit at 0.75° and the receiving slit at 0.2mm. This gives an instrument resolution of 0.15°. The second diffractometer was a Philips $\theta - 2\theta$ diffractometer which also had a copper target x-ray tube. In this geometry, the tube position is kept fixed while the sample and detector are rotated through angles of θ and 2θ respectively. The slits in this machine were set at 0.5° for the divergence slit and 0.2mm for the receiving slit. This also gives an instrument resolution of 0.15°. Both diffractometers had diffracted beam monochromators to eliminate fluorescence which emanates from

transition metals like iron. The fluorescence occurs from the absorption of x-rays by the iron oxide followed by the re-emission of x-rays at a different wavelength.

In preparation for the x-ray diffraction study, the samples were ground for a minimum of 15 minutes to produce fine powders. The powder sample to be measured was then pressed into a stainless steel well holder.

4.2 Rietveld Refinement

The Hill and Howard version of the Rietveld program was used. The program calculates an x-ray diffraction patterns according to (Hill and Howard, 1985).

$$y_{ic} = y_{ib} + \sum_{k=k_1}^{k_2} G_{ik} I_k \tag{4-1}$$

where y_{ic} is the intensity calculated at point i in the pattern. Point i corresponds to a 0.05°step, y_{ib} is the background intensity calculated by the program, G_{ik} is a normalized peak profile function determining the half width and the shape of the peak (Lorentzian/Gaussian), I_k is the intensity of the k^{th} Bragg reflection and $k_1 ... k_2$ are the reflections contributing intensity to point i.

The intensity I_k is determined from (Cullity, 1978, Hill and Howard, 1985)

$$I_k = S M_k L_k |F_k|^2 P_k \tag{4-2}$$

where S is a scale factor, M_k is the multiplicity, L_k is the Lorentz-polarization factor, F_k is the structure factor and P_k is the preferred orientation parameter which is set to one when there is no preferred orientation of the powder grains. The origin of all these terms will

discussed in section 4.2.1. The calculated pattern is compared to the measured data and the program adjusts the structural parameters to minimize the difference between the measured and calculated patterns.

4.2.1 Calculating Peak Intensities

The intensity of a powder x-ray diffraction peak is given by equation 4-3 (Cullity, 1978):

$$I = |F|^2 M\left(\frac{1+\cos^2 2\theta \cos^2 2\theta_m}{\sin^2\theta\cos\theta}\right)S \qquad (4\text{-}3)$$

Where F is the structure factor, M is the multiplicity factor, 2θ is the scattering angle from the sample and $2\theta_m$ is the scattering angle from the monochromator. The term in brackets is the Lorentz-polarization factor. The preferred orientation term, P, has been set to one. The intensity, I, refers to the integrated intensity from a particular Bragg peak.

The incoming x-rays are scattered from the electrons in the material. The electrons are situated at different points in space around the atoms thereby introducing phase differences between the waves scattered by different electrons of each atom. Thus the scattered intensity is dependent on the type of atom. For a particular atom, an atomic form factor, *f*, has been defined by Cullity as:

$$f = \frac{\text{amplitude of wave scattered by an atom}}{\text{amplitude of wave scattered by one electron}}$$

and described as the "efficiency of scattering of a given atom in a given direction" (Cullity, 1978).

The International Tables (1969) define f by equation 4-4

$$f(\lambda^{-1}\sin\theta) = \sum_{i=1}^{4} a_i \exp(-b_i\lambda^{-2}\sin^2\theta) + c \qquad (4\text{-}4)$$

where a_i, b_i and c, found in the International Tables, are coefficients that fit the results of the analytic expression in 4-4 to scattering factors calculated by ab-initio methods.

Now we consider how the x-rays scattered from different atoms interact with one another. In order to take this interaction into account the position of the different atoms in the unit cell must be known.

$LiFeO_2$ and $NaFeO_2$ have a hexagonal unit cell with cell dimensions given in Table 1. The space group for the system is $R\bar{3}m$. The fractional atomic coordinates, in the hexagonal setting are:

Fe: (000); (1/3 2/3 1/3) ; (2/3 1/3 2/3)
Li/Na: (001/2); (1/3 2/3 5/6); (2/3 1/3 1/6) and
O: $\pm$(00z); $\pm$(1/3 2/3 z+1/3); $\pm$(2/3 1/3 z+2/3)

where z was initially set to 1/4.

Using these fractional atomic coordinates for lithium, iron and oxygen atoms and knowing the atomic form factors for each of these atoms, it is possible to calculate the structure factor, F, for the unit cell. The structure factor describes how the arrangement of the atoms, given by the fractional atomic coordinates, affects the scattered beam. If a unit cell has N atoms, each with fractional coordinates u_1, v_1, w_1, ..., u_N, v_N, w_N and

atomic scattering factors $f_1, f_2, \ldots, f_N$ then the structure factor is defined by equation 4-5 (Cullity, 1978)

$$F=f_1 \exp\{2\pi i(hu_1 + kv_1 + lw_1)\} + \ldots + f_N \exp\{2\pi i(hu_N + kv_N + lw_N)\} \qquad (4\text{-}5)$$

where hkl are the Miller indices which are determined below.

The Lorentz-polarization term

$$\frac{1+\cos^2 2\theta}{\sin^2 \theta \cos\theta} \qquad (4\text{-}6)$$

will be discussed next. The numerator in expression 4-6 is the polarization term. It comes from the Thomson equation (4-7) for the scattering of an x-ray beam by a single electron. For unpolarized x-rays striking an electron at the origin, the intensity measured at some point P is given by (Cullity, 1978)

$$I_P = I_O \frac{K}{r^2}\left(\frac{1+\cos^2 2\theta}{2}\right) \qquad (4\text{-}7)$$

where I_O is the intensity of the incident beam, K is 7.94×10^{-30} m^2, r is the distance between the point of measurement and the electron from which the x-rays are scattered and 2θ is the angle between the incident and scattered beams. Similarly, the reflections from the monochromater crystal contribute a term proportional to $\cos^2 2\theta_m$.

In most cases, all factors on the right hand side of equation (4-7) are constant except the last one. This last factor, which takes the form $\frac{1+\cos^2 2\theta \cos^2 2\theta_m}{2}$ when the monochromator is taken into account, is called the polarization factor.

The denominator in expression (4-6) ($\sin^2\theta\cos\theta$) is the Lorentz term and it arises from geometrical factors particular to the powder method (Cullity, 1978).

The remaining factor in the intensity equation given in equation (4-3) is M, the multiplicity factor. The multiplicity factor is the sum of the number of Bragg planes which contribute to the same reflection. For the cubic system of {100} planes, the multiplicity is 6. For the hexagonal system of {110} Bragg planes, the multiplicity is 6.

The intensity equation is a function of the angle between the incident and scattered x-ray beams, 2θ. X-ray beams scattered from an electron can be scattered in all directions. However constructive interference between these scattered beams only occurs at particular angles. The condition for constructive interference, for rays scattered from atoms in parallel layers, is Bragg's law which requires that the path difference between scattered waves must be an integral number of wavelengths:

$$n\lambda = 2d\sin\theta \qquad (4\text{-}8)$$

where λ is the wavelength of the incident x-rays, θ is the angle between the incoming radiation makes with the plane doing the scattering, d is the distance between parallel Bragg planes and n=1.

The scattering vector is defined as the difference between the incoming vector and the reflected vector:

$$\vec{q} = \vec{k} - \vec{k}' \tag{4-9}$$

where

$$q = \frac{4\pi \sin\theta}{\lambda} = \left\| h\vec{b}_1 + k\vec{b}_2 + l\vec{b}_3 \right\| \tag{4-10}$$

and $\vec{b}_1$, $\vec{b}_2$ and $\vec{b}_3$ are the reciprocal lattice vectors.

For the hexagonal system,

$$q = \{h^2 b_1^2 + k^2 b_2^2 + l^2 b_3^2 + 2hk(\vec{b}_1 \cdot \vec{b}_2)\}^{1/2} \tag{4-11}$$

where $|b_1| = |b_2|$, so q can be re-expressed as:

$$q = \{b_1^2(h^2 + k^2 + hk) + l^2 b_3^2\}^{1/2} \tag{4-12}$$

Solving for θ, an equation involving the Miller indices is obtained

$$\theta = \sin^{-1}\{\frac{\lambda}{4\pi}[b_1^2(h^2 + k^2 + hk) + b_3^2 l^2]^{1/2}\} \tag{4-13}$$

There are other factors that affect the relative intensity of the Bragg peaks. The first is the temperature factor. So far, the intensity calculation has been based on scattering from stationary atoms in a lattice. Since atoms actually vibrate about their mean positions, it is necessary to consider the effect of these vibrations. Thermal

vibrations smear out the planes in the lattice, thereby decreasing the intensity of a diffracted beam (Cullity, 1978). The intensity of a diffracted beam decreases as the temperature is increased since the increase in temperature causes an increase in the amplitude of the vibrations. For a particular temperature, the thermal vibrations cause a greater decrease in the reflected intensities at higher angles (Cullity, 1978).

The other factor which may affect the intensity is whether or not a site in the lattice is occupied by an atom. In a perfect crystal, all the sites in the lattice would be occupied by the appropriate atoms, as designated by the atomic coordinates on page 28. Since the powders synthesized in this study are by no means synthsized in ideal condition, there could be lattice defects leading to unoccupied sites, or even perhaps lithium on the iron sites and iron on the lithium sites.

The Rietveld program is capable of varying the site occupancy of any of the atoms. However in order to prevent the program from crashing, it was necessary to fix the site occupancy of the oxygen. The program is also capable of placing some concentration of lithium on iron sites, and vice versa.

The Rietveld program calculates the intensity of a Bragg peak using the method outlined above.

4.2.2 Comparison to Measured Data

Section 4.2.1 describes the steps necessary to calculate the integrated intensity of a particular Bragg peak. Thus far, no shapes have been assigned to these peaks. From equation 4-1, the peak shape profile is given by G_{ik} which, for a peak which can be Lorentzian or Gaussian or some combination thereof, is given by (Rietveld):

$$G_{ik} = \gamma \frac{C_o^{1/2}}{H_k \pi}[1 + C_o X_{ik}^2]^{-1} + (1-\gamma)\frac{C_1^{1/2}}{H_k \pi}\exp[-C_1 X_{ik}^2] \qquad (4\text{-}14)$$

where C_o=4, C_1=-4ln2, H_k is the full width at half maximum (FWHM) of the k^{th} Bragg reflection, $X_{ik} = \frac{(2\theta_i - 2\theta_k)}{H_K}$ and γ is a refinable mixing parameter which for a pure Gaussian peak is equal to 0 and for a purely Lorentzian peak is given by $\gamma = 1$. The FWHM parameter H_k is given by:

$$H_k = (U\tan^2\theta + V\tan\theta + W)^{1/2} \qquad (4\text{-}15)$$

where U, V and W are refinable parameters and θ is the Bragg angle defined in (4-13)

The Rietveld program can also calculate a background intensity, $y_{ib,}$ in order to improve the agreement between the measured and calculated profiles. The value of y_{ib} is given by:

$$y_{ib} = \sum_{m=-1}^{4} B_m (2\theta_i)^m \qquad (4\text{-}16)$$

where B_m is one of six refinable parameters.

The Rietveld program can simultaneously vary the lattice parameters, the background, the thermal factor, the atomic coordinates, the site occupations and FWHM, and the Lorentzian/Gaussian ratio for all the peaks in the specified angular range.

The program calculates an intensity for each 0.05° step in the profile and compares each of these calculated values to the measured data. The result is a goodness of fit, G.O.F, or χ^2, from equation 4-17.

$$\chi^2 = \frac{\sum_i w_i(y_{io} - y_{ic})^2}{N - P} \tag{4-17}$$

where w_i is the weighting factor assigned to individual step intensities. It is the reciprocal of the variance σ^2

$$w_i = \frac{1}{\sigma^2} = \frac{1}{y_{ic}} \approx \frac{1}{y_{io}} \tag{4-18}$$

where y_{io} is the observed or measured intensity for each 0.05° step, y_{ic} is the calculated intensity for each 0.05° step, N is the number of observations and P is the number of adjusted parameters. The program works to minimize χ^2.

In order to quantify the fit between the measured and calculated peaks, the Rietveld program calculates a Bragg R factor, R_B, defined as:

$$R_B = \frac{\sum_k |I_{ko} - I_{kc}|}{\sum_k I_{ko}} \tag{4-19}$$

where I_{ko} is the observed or measured intensity for the k^{th} Bragg peak and I_{kc} is the calculated intensity for the same peak.

The parameters just described are those that are typically varied by the Rietveld program. However, there are other optional parameters which may be varied. Normally an overall isotropic vibration is assigned to all the different atoms in the unit cell. Sometimes, it is necessary to replace the overall isotropic temperature factor, characterizing the whole material, with individual isotropic parameters, dependent on the atom. An isotropic temperature factor is characterized by a sphere, representing isotropic movement. However if an atom is moving preferentially in one direction because of its confining structure, the movement can no longer be represented by a sphere, but instead by oblate spheroids, ellipses, etc.. This may be the case in $LiFeO_2$ and $NaFeO_2$ and so this behaviour was incorporated into the refinement program.

The other optional parameter which may be varied in order to improve the fit is preferred orientation. In some materials, each grain in the powder will have a crystallographic orientation different from that of its neighbours. As a result, the crystallite orientations are randomly distributed. However, in other materials, grains may cluster about some particular orientation. Any grouping of this sort is said to have a preferred orientation, that is a non-random distribution of crystal orientation. This non random distribution will result in an x-ray diffraction pattern that has directional dependence. This parameter will attempt to characterize the preferred directions.

4.3 STRUCTURAL RESULTS FOR MATERIALS MADE

The $NaFeO_2$ powder, produced via the procedure described in chapter two, was examined by x-ray diffraction to check that the alpha phase had been formed. The

expected reflections, with their corresponding scattering angle for the hexagonal system, obtained from a CD-ROM data base (JCPDS), are given in Table 2.

Table 2: The Miller indices, scattering angles and peak intensities for $NaFeO_2$

h k l	Scattering Angle	Intensity (Expected)	Intensity(Measured)
0 0 3	16.525	30	73
0 0 6	33.407	8	13
1 0 1	34.673	30	17
0 1 2	36.025	55	30
1 0 4	41.068	100	100
0 1 5	44.553	2	3
1 0 7	52.977	4	7
0 1 8	57.715	10	17
1 1 0	61.209	40	24
1 1 3	63.881	8	4

The measured pattern for $NaFeO_2$ is shown in Figure 4-1, with indexed peaks and agrees well with the expected pattern in Table 2. All the expected peaks, with the right intensity ratios, and no others are observed, so the alpha phase of $NaFeO_2$ was synthesized.

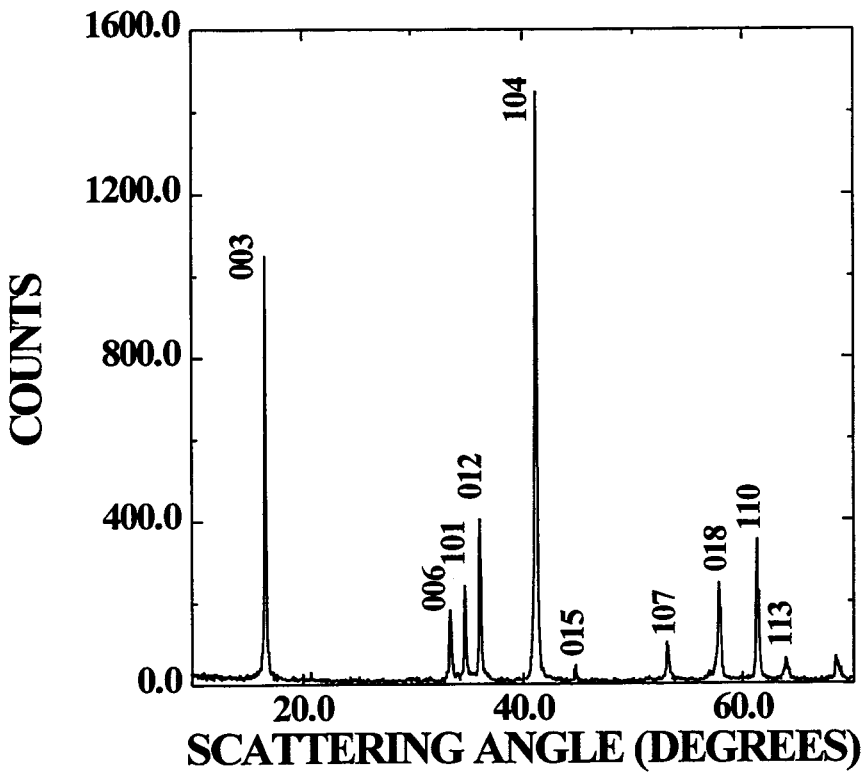

Figure 4-1: Measured x-ray diffraction data for $NaFeO_2$

The $NaFeO_2$ powder is then ion exchanged with $LiNO_3$, as described in chapter two, to produce $LiFeO_2$. The $LiFeO_2$ powder produced was similarly examined by x-ray diffraction. The expected scattering angles and Miller indices for Bragg peaks for $LiFeO_2$, obtained from CD-ROM data base (JCPDS), are listed in Table 3.

Table 3: The Miller indices, scattering angles and peak intensities for $LiFeO_2$.

h k l	Scattering Angle	Intensity (Expected)	Intensity(Measured)
0 0 3	18.277	100	100
1 0 1	35.597	44	50
0 1 2	37.264	14	23
1 0 4	43.166	60	73
0 1 5	47.175	10	11
0 0 9, 1 0 7	56.935	12	11
1 1 0	62.821	30	37
1 1 3	66.016	12	11

The measured pattern for $LiFeO_2$ is shown in Figure 4-2, with indexed peaks. As was the case for $NaFeO_2$, all the predicted peaks and no others are observed.

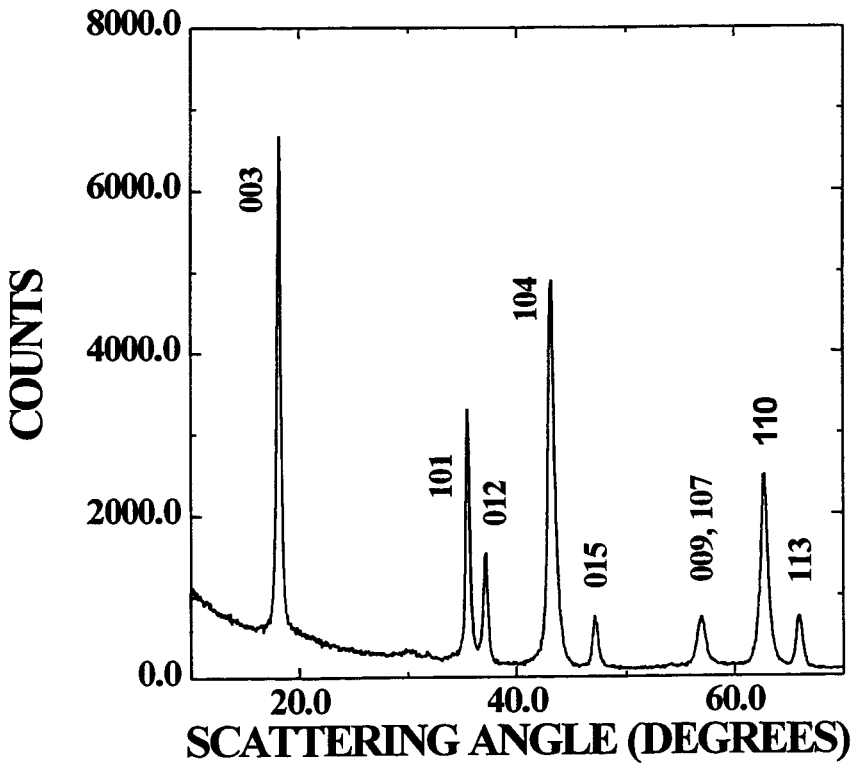

Figure 4-2: Measured x-ray diffraction data for $LiFeO_2$

The cobalt-doped sodium iron oxide pattern is shown in Figure 4-3A. The synthesis appears to have proceeded successfully. The corresponding lithium compound is shown in Figure 4-3B. The materials have phase separated since new peaks have appeared in the pattern, at the peak positions for $LiCoO_2$. The peak positions and Miller indices for $LiCoO_2$, obtained from CD-ROM database (JCPDS), are given in Table 4.

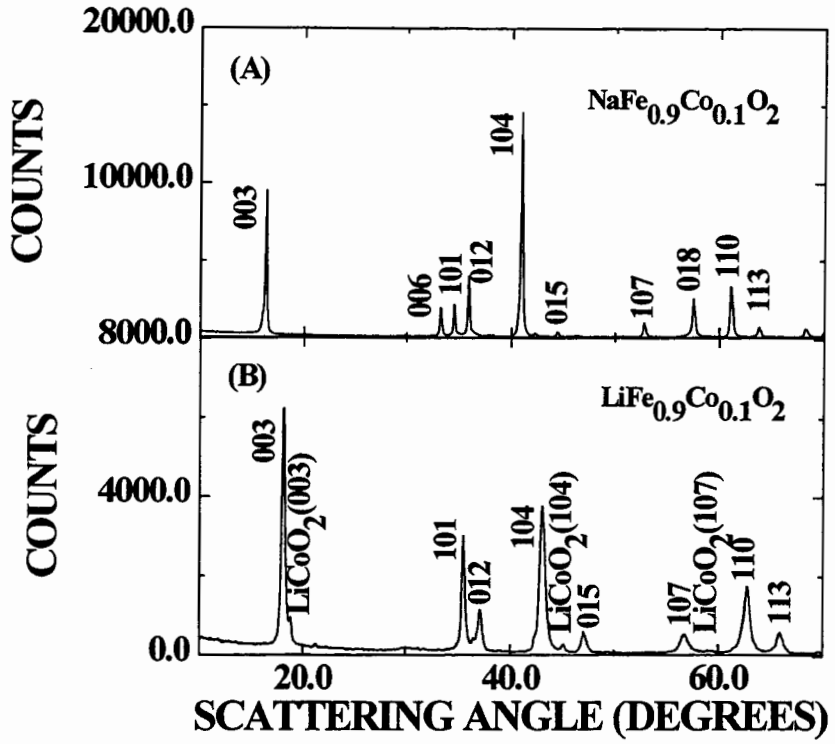

Figure 4-3(A): X-ray diffraction pattern for cobalt containing sodium iron oxide material; (B): X-ray diffraction pattern for cobalt containing lithium iron oxide

Table 4: The Miller indices, scattering angles and peak intensities for $LiCoO_2$.

h k l	*Scattering Angle*	*Intensity (Expected)*
0 0 3	*18.947*	*100*
1 0 1	*37.425*	*16*
0 0 6	*38.336*	*4*
0 1 2	*39.098*	*4*
1 0 4	*45.281*	*35*
0 1 5	*49.468*	*6*
1 0 7	*49.640*	*10*
0 1 8	*65.494*	*10*
1 1 0	*66.386*	*8*
1 1 3	*69.699*	*6*

Figures 4-4A and 4-4B show the x-ray diffraction patterns for the nickel and chromium doped sodium iron oxide samples. As stated in chapter two, the synthesis did not proceed successfully, but instead produced $NaFeO_2$ and NiO for the nickel doped material, or $NaFeO_2$ and unknown phases for the chromium doped material.

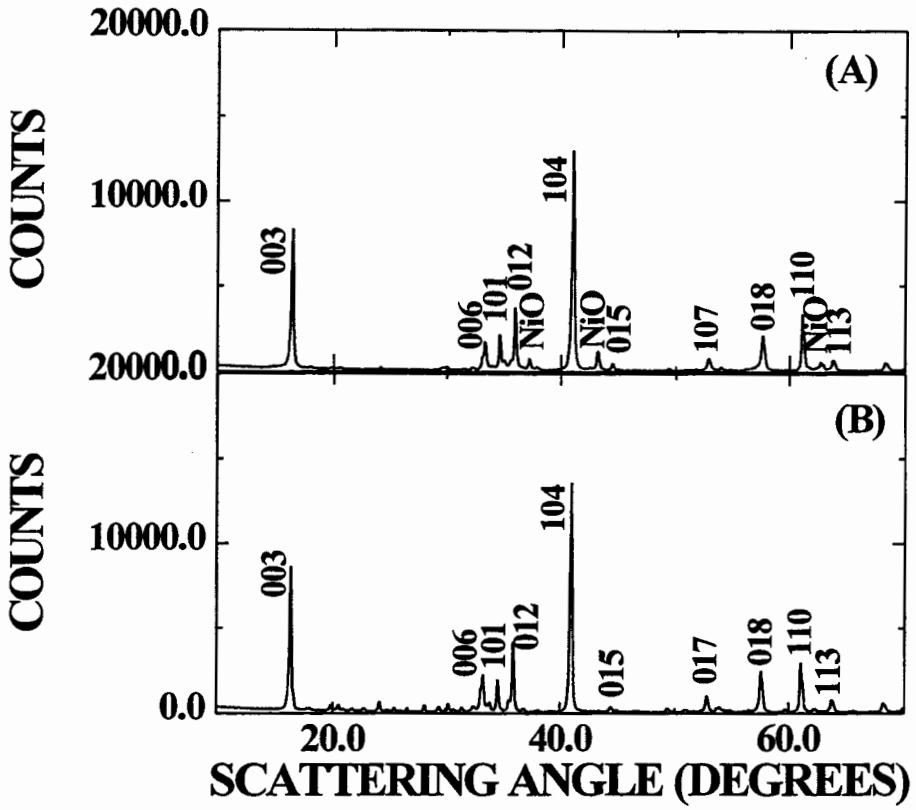

Figure 4-4(A): X-ray diffraction pattern for nickel doped $NaFeO_2$;(B): x-ray pattern for chromium doped $NaFeO_2$

The x-ray diffraction studies indicate that the $NaFeO_2$ and $LiFeO_2$ powders were successfully synthesized. At this point, the Rietveld program was used to compare the measured diffraction pattern with that calculated by the program. This comparison allows the determination of the actual lattice parameters, site occupancies, temperature factors, etc.., within an error range determined by the goodness of fit of the profile.

The parameters obtained from the Rietveld program for both the $NaFeO_2$ and $LiFeO_2$ materials are listed in Table 5. They were obtained without using anisotropic temperature factors and without preferred orientation.

Table 5: The unit cell parameters obtained from the Rietveld refinement program for $LiFeO_2$ and $NaFeO_2$

	a & b (Å)	c (Å)	Li/Na conc.	Fe conc.	Bragg R	G.O.F
$NaFeO_2$	3.0245±0.0002	16.0882±0.0016	1.04462	.94438	7.42	1.83
$LiFeO_2$	2.9501±0.0005	14.5256±0.0016	.8244	.8756	5.21	2.34

For $NaFeO_2$, the measured and calculated patterns are compared pictorially in Figure 4-5. The lower panel on the graph shows the difference between the two patterns. As listed in Table 5, the G.O.F yields a 1.83.

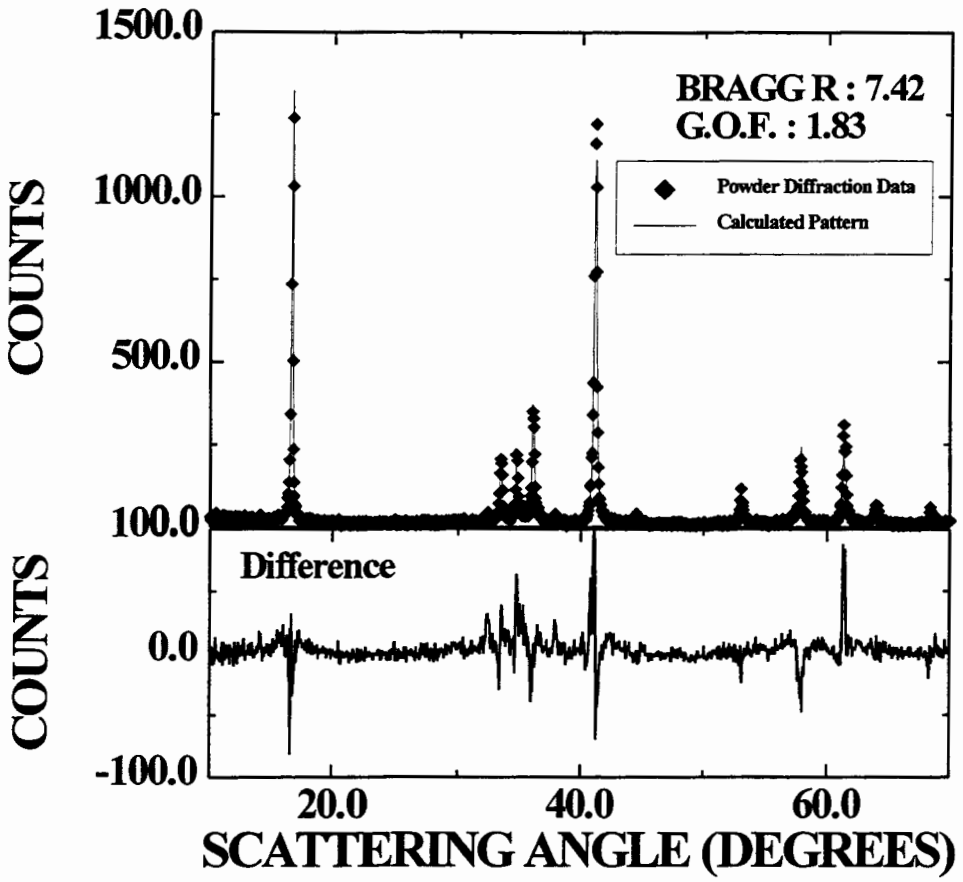

Figure 4-5: Rietveld refinement obtained for $NaFeO_2$, compared with measured pattern

For $LiFeO_2$, the measured and calculated patterns are shown in Figure 4-6. The G.O.F. is 2.34.

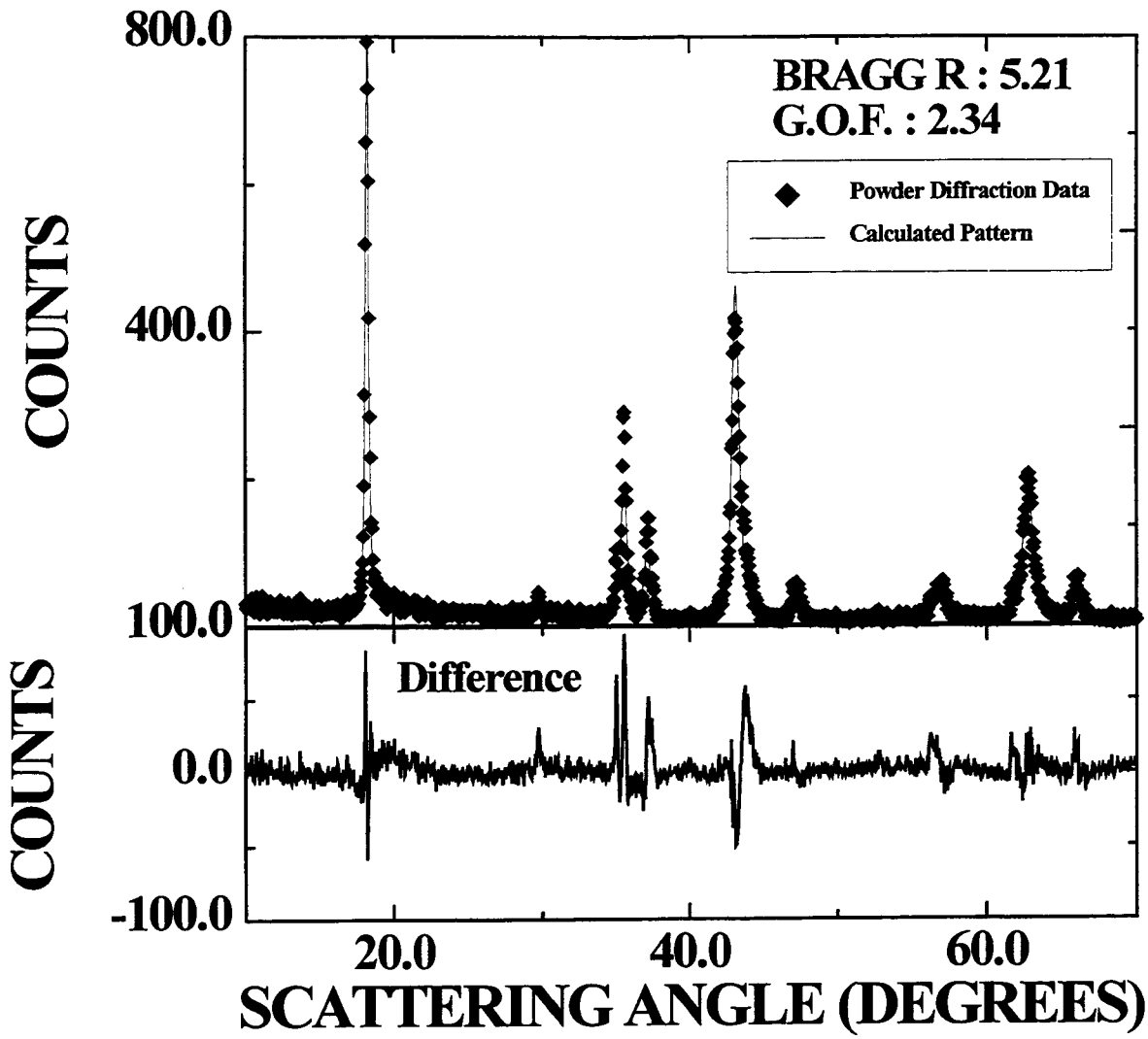

Figure 4-6: Rietveld refinement obtained for $LiFeO_2$ compared with measured pattern

These fits show that the desired layered phase of the material was produced. However, attempts were made, using the anisotropic temperature factor and preferred orientation, to improve these results. The resulting G.O.F. and Bragg R values are listed for $NaFeO_2$ in Table 6.

Table 6: The Goodness of Fit and Bragg R values for $NaFeO_2$ obtained from the Rietveld refinement program when anisotropic temperature factors and preferred orientation parameters were added.

Refinement	G.O.F	Bragg R
$NaFeO_2$ - Base Refinement	1.83	7.42
$NaFeO_2$ - with anisotropic temperature factor added	1.79	5.80
$NaFeO_2$ - with preferred orientation added	1.79	5.79
$NaFeO_2$ - with anisotropic temperature factor and preferred orientation added	1.79	5.60

The addition of preferred orientation or anisotropic temperature factors does not yield any improvement to the overall fit but it does slightly improve the Bragg R, and thus the fit of the peak intensities. The powders were deemed not to have preferred orientation, and not to exhibit anisotropic temperature behavior.

CHAPTER FIVE

5. EXPERIMENTAL - PART III: ELECTROCHEMICAL PROPERTIES

5.1 Introduction to Electrochemical Methods

The main aim of this project was to study the electrochemical behavior of layered iron oxide materials. Assuming the lithium can be reversibly de-intercalated from the iron oxide in question, then electrochemical measurements made on a cell which has lithium metal as a reference anode provides a relatively easy, yet sensitive, method to study the behavior of these materials. In an electrochemical study, the concentration of lithium contained in an electrode at any given time while the experiment is running is constantly changing. The test used in this study used a constant current to cycle , that is charge and discharge, the cells between upper and lower voltage limits.

5.1.1 Chemical Potential

As mentioned in the introduction, on discharge lithium ions dissolve in the electrolyte and travel to the transition metal oxide. This spontaneous occurrence is the basis of lithium transition metal oxide cells. The process occurs because lithium has a lower chemical potential in the TMO than it does in the lithium metal.

The chemical potential of a material is defined by equation 5-1 (Way, 1995)

$$\mu = \frac{dG}{dn} \qquad (5\text{-}1)$$

where G is the Gibbs Free Energy and n is the number of transferred atoms.

The spontaneous dissolution of z lithium ions into the electrolyte is accompanied by the movement of z electrons though the outer circuit. The electrons are available to do work. They then reunite with the lithium ions at the TMO surface and diffuse though the lattice. The change in free energy for both electrodes, defined per ion, is:

$$\Delta\mu = \mu_{cath} - \mu_{anode} \tag{5-2}$$

Work is done by the corresponding electrons

$$W = -zeV \tag{5-3}$$

where V is the voltage across the electrodes. Ignoring losses, the change in free energy of the lithium, as it travels from the anode to the cathode, equals the work done by the electrons in the external circuit. Then

$$V = \frac{-(\mu_{cath} - \mu_{anode})}{e} \tag{5-4}$$

which is an equilibrium expression for the voltage as a function of the chemical potential of lithium in both electrodes.

For the purpose of the electrochemical studies performed during this study, unless otherwise indicated, the anode is lithium metal. Hence, the anode is of a homogeneous phase and so the chemical potential of the lithium in the anode is constant.

The resulting cell then has an anode with constant chemical potential and a cathode whose chemical potential varies as a function of lithium content. As a result, the

voltage is a direct measurement of the chemical potential of the lithium in the cathode as a function of the lithium content.

5.2 **Cell Construction and Testing**

There are several steps involved in the process of cell construction and testing, including electrode fabrication, cell assembly and finally cell testing. This section will discuss the processes involved step by step.

5.2.1 Electrode Fabrication

The electrode of interest in this study was the cathode composed of the iron oxide materials $NaFeO_2$ or $LiFeO_2$, which were synthesized as indicated in chapter two. The anode to be used in the electrochemical studies was a 125 μm thick lithium foil, which was supplied to the lab by Moli Energy (1990) Ltd.. Lithium is extremely reactive with air, as a result the actual process of cell construction must proceed in an argon glovebox.

Cathode preparation proceeds as follows. The iron oxide powder to be studied is ground into a fine powder by an autogrinder. Some of this finely ground powder is placed into a mortar, and about 10% by mass of Super S Carbon Black (from MMM Carbon) is then added to the iron oxide. The two are lightly ground together, with mortar and pestle, in order to ensure a good mixture. The carbon black is filamentous and acts to maintain electrical contact between all the grains in the material. This mixture of iron oxide and Super S is placed into a plastic shaker bottle to which is added a 3.87% EPDM binder solution. Enough binder solution is added to the mixture so that the final mass of the material contains roughly 3% EPDM. Cyclohexane is then added to the shaker bottle

in order to thin it out and make a slurry. The bottle is shaken until a good mixture is obtained, roughly 10 minutes. At this point, if the consistency is too runny, the top is left off the bottle and some of the cyclohexane is left to evaporate. Once the mixture has attained the desired consistency, it is poured into a doctor blade spreader, gapped at 12 thousandths of an inch, and spread onto a strip of aluminum foil. The result is a strip of iron oxide cathode material, which is left to dry in air for 15 minutes. The cathode is lightly bound to the aluminum foil and is ready to use. It should have a thickness of between 100-200 μm. This strip of electrode material is cut into 1.2cm x 1.2 cm squares which are the right size for the cell hardware. The mass of the square is measured and the mass of active material determined. The active mass refers to the actual mass of the iron oxide material in the cathode. On average it was found that the aluminum foil of 1.2cm x 1.2cm dimensions weighed 8.5mg. With this knowledge, the active mass of material in the cathode can be determined.

$$\text{active mass} = \{\text{mass cathode} - \text{average foil mass}\} \times \%\ \text{active material in slurry} \quad (5\text{-}5)$$

Recall that the slurry is composed of Super S, iron oxide, EPDM binder and cyclohexane. The cyclohexane evaporates so it is not incorporated into the calculation for the percent active mass in the slurry.

$$\%\ \text{active material} = \frac{\text{mass iron oxide}}{\{\text{mass iron oxide} + \text{mass Super S} + \text{mass (EPDM}*3.87\%)\}} \quad (5\text{-}6)$$

The latter is multiplied by 3.87% since the EPDM binder is a solution. However once the cathode is dry, all that remains is the 3.87% EPDM contained in the original solution. The mass of iron oxide in the cathode can then be determined.

The lithium metal anodes are also cut into 1.2cm x 1.2cm squares.

5.2.2 Cell Assembly

Having cut the cathodes into the 1.2cm x 1.2cm squares, cell assembly is ready to proceed to the glove box. The cell hardware components are the top and bottom casing of a 2320 type coin cell (23mm diameter, 2.0mm thickness) with a polypropylene gasket, the two electrodes, a microporous 50 micron thick polypropylene separator, a stainless steel spacer and a stainless steel disc spring.

Cell assembly proceeds, in an argon filled glove box, as shown in Figure 5-1

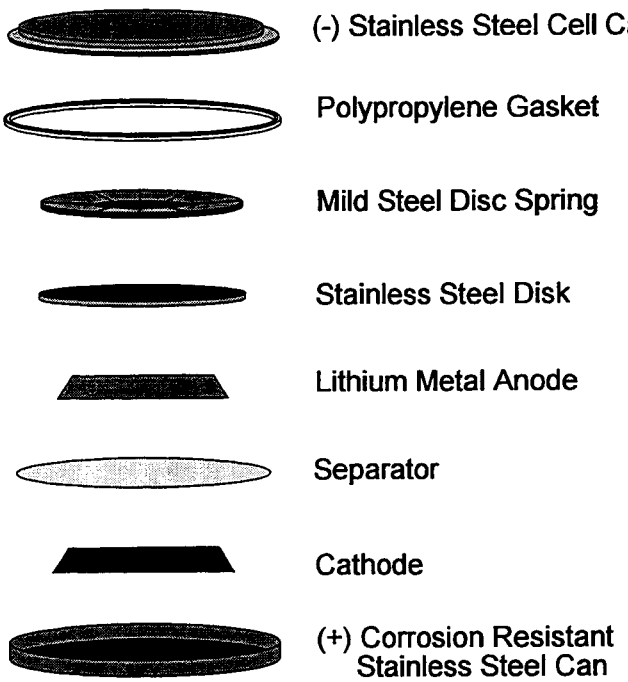

Figure 5-1: Exploded view of coin cell (Way, 1995)

The electrolyte used was 1M $LiPF_6$ salt in a 30/70 (v/v) mixture of ethylene carbonate (EC)/diethyl carbonate(DEC). The structures for the two components are shown in Figure 5-2.

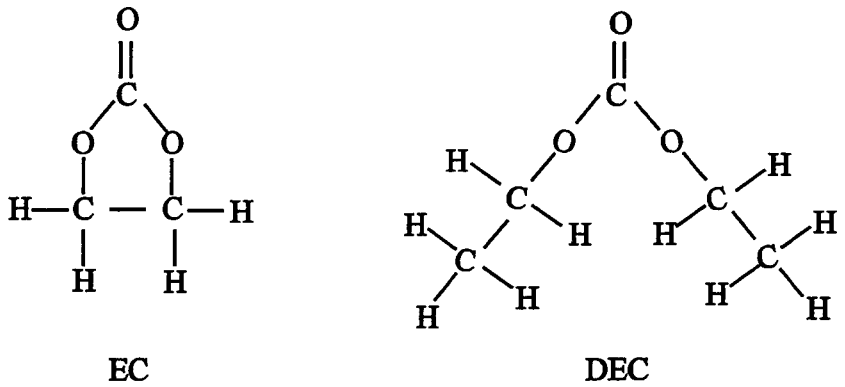

Figure 5-2: Schematic drawing of the structure of EC and DEC (Zheng, 1996)

The cathode is placed on the bottom of the can. Five to six drops of electrolyte are placed on top of the cathode and the separator is placed above the cathode. The separator absorbs the electrolyte. Sufficient electrolyte needs to be added to the cell in order for the separator to become clear. The precut lithium metal foil is then placed above the separator and lined up so that it is directly above the cathode. The spacer is placed next and then the disc spring. The spring will apply pressure to the electrode separator combination in order to ensure good electrical contact. Finally the cell cap is placed.

The components are then placed into a press and 2500 pounds of force applied in order to fold the edge of the can over the side of the cap. The cell is now sealed from the environment and is ready to be removed from the glove box. Stainless steel tabs are then spot welded onto the outside of the can. These will act as current collectors.

Cells were tested using a computer controlled charger system obtained from Moli Energy (1990) Ltd. The program allows the voltage and current set point for individual cells to be programmed and sent to the individual charger boards. Voltages are measured by an integrated Keithley 196 voltmeter. The temperature of the cells is monitored and kept at a constant 30 ± 1 °C.

5.3 Results

5.3.1. $NaFeO_2$

The electrochemical behaviour of both $NaFeO_2$ and $LiFeO_2$ was examined. The results for $NaFeO_2$ are shown in Figure 5-3. The figure shows a voltage curve for the material. A voltage curve is obtained when the cell is cycled at constant current between upper and lower voltage trip points. During charge, a current source is used to provide a constant current until the measured cell voltage exceeds the upper trip voltage, at which time the current direction is reversed and the cell is discharged to the lower voltage trip point. The voltage is measured as a function of time.

The current to be used was input into the program prior to cell testing. The current is dependent on the hour rate desired. The hour rate, H.R., is the amount of time until a full charge or discharge is complete.

$$I = \frac{C_S * A.M.}{H.R.} \qquad (5\text{-}7)$$

where C_s is the specific capacity of the material in mAh/g, calculated for the case when all the lithium is removed, and A.M. is the active mass of the material calculated as shown in equation 5-5.

$$C_S = \frac{F}{3600\text{mAh} / C * \text{M.W.}} \tag{5-8}$$

where F is Faraday's number, 96480 C/mole, and M.W. is the molecular weight, in g/mole, of the material being studied.

For $NaFeO_2$, there is a plateau on charge between 3.95V and 4.7V. However on discharge, the corresponding plateau, indicating some atoms are returning to the lattice, is not present. The reason for this is unclear.

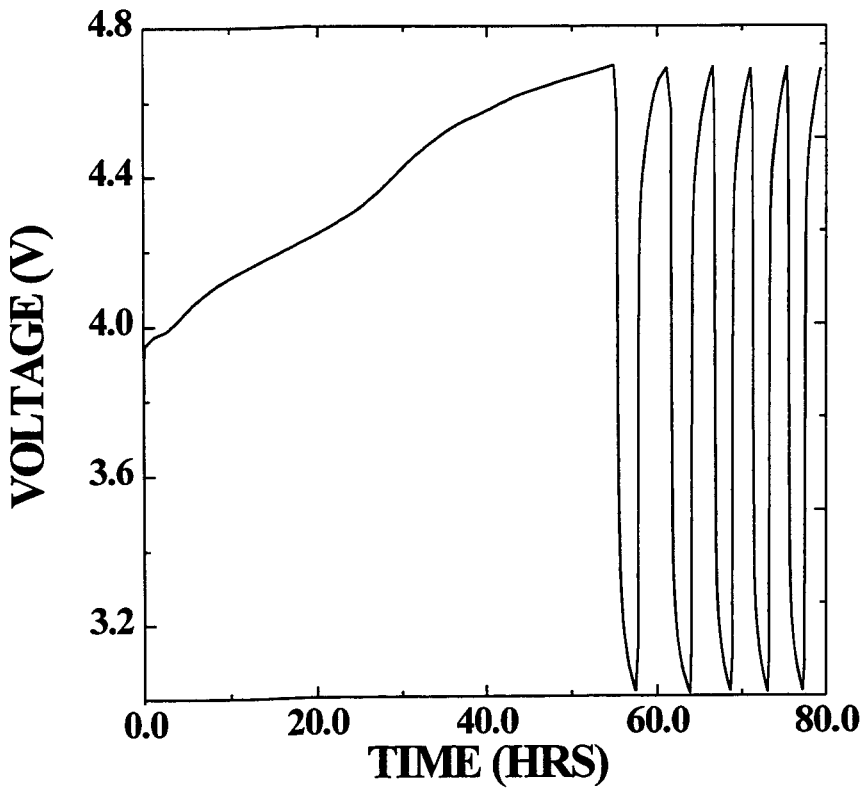

Figure 5-3: Voltage curve for $NaFeO_2$.

For layered materials of this type, if intercalation is occurring one would expect a voltage curve similar to that of $LiNiO_2$ shown in Figure 5-4. The charge and discharge parts of the curve are almost identical.

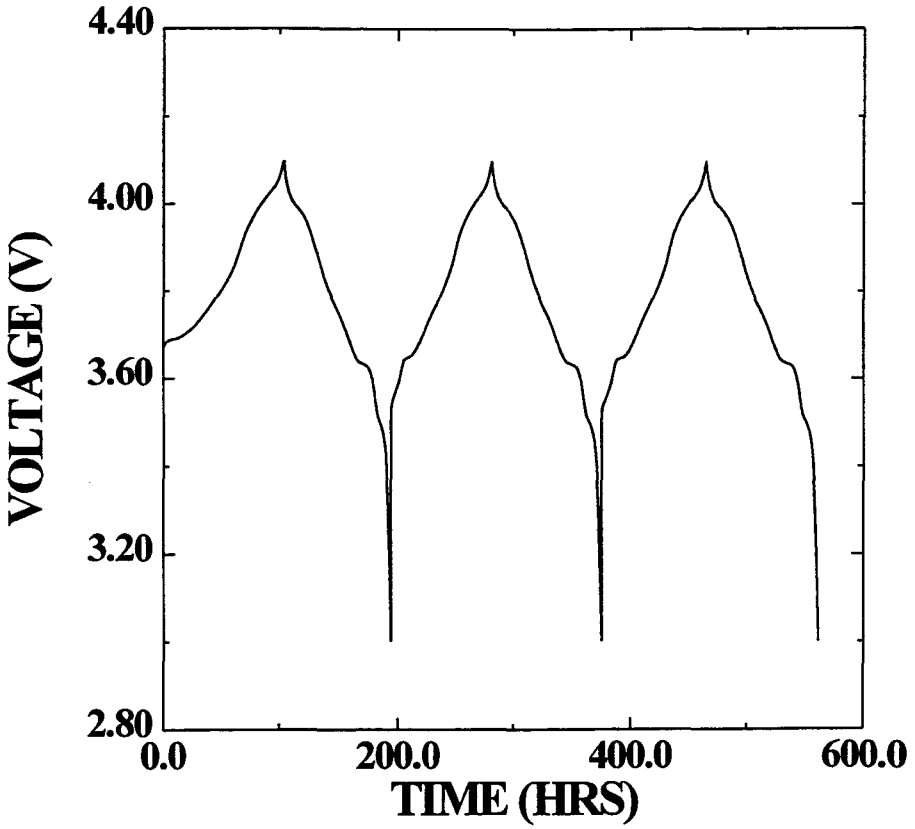

Figure 5-4: Voltage curve for $LiNiO_2$.

5.3.2 $LiFeO_2$

For $LiFeO_2$ a voltage curve is shown in Figure 5-5. The $LiFeO_2$ cell was also cycled at a 100 hour rate, however the charge only lasted approximately 7 hours, indicating very little lithium is removed. The plateau is between 4.3V and 4.7V. As in the case of $NaFeO_2$ voltage profile, there is no corresponding plateau on discharge. The reason for this is unclear.

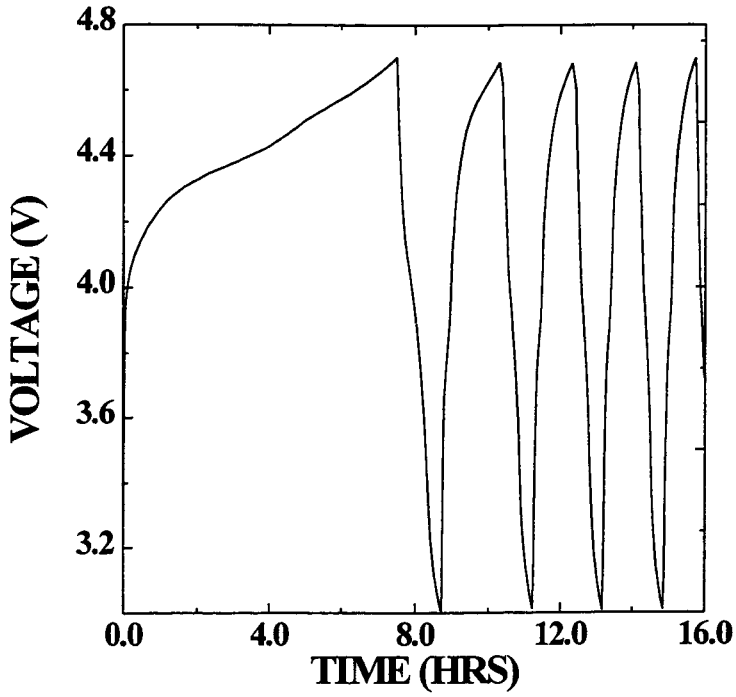

Figure 5-5: Voltage curve for $LiFeO_2$

The behaviour of the $NaFeO_2$ and $LiFeO_2$ materials is unexpected. In the $LiFeO_2$ material, so little lithium is removed and none of it is returned. In the $NaFeO_2$ materials, it seems sodium atoms are removed, however no lithium enters the structure on discharge. These phenomena are mysterious and in an attempt to understand them in-situ x-ray studies were carried out.

CHAPTER SIX

6. EXPERIMENTAL - PART IV: IN-SITU DIFFRACTION STUDIES

6.1 In-Situ X-Ray Cells and Diffraction

The electrochemical behaviour of the $NaFeO_2$ and $LiFeO_2$ is unexpected. In the case of $NaFeO_2$, the voltage profile shows what appears to be the removal of sodium atoms on charge. However, the discharge process does not show the re-insertion of the sodium or lithium atoms into the iron oxide lattice. The behaviour of $LiFeO_2$ is somewhat similar. On charge, there appears to be only a small amount of lithium removed from the iron oxide lattice. The amount of lithium removed was much smaller than expected and on discharge it does not return to the lattice.

There are problems with each of the materials, whose sources can possibly be determined by in-situ x-ray diffraction measurements. This chapter will discuss the processes of electrode fabrication, cell construction and cell testing.

6.1.1 Electrode Fabrication

The electrodes are of the same type as described in section 5.2.1. They are a mixture of sodium/lithium iron oxide powder, Super S carbon black and EPDM binder , to which cyclohexane is added in order to make the solution of a desired consistency. The resulting mixture is poured into a doctor blade spreader and a thin film is spread on an aluminum substrate. Once the cyclohexane has evaporated the dried film is cut into 1.2x1.2 cm squares using a precision cutting jig. The anode is lithium metal, also cut into 1.2 x 1.2 cm squares.

6.1.2 Cell Assembly

In-situ cells must be designed to allow x-rays to reach the material to be studied, which in this case is the cathode material. The cell design in this study uses a beryllium window which is placed inside a cell can that has a hole punched in it. The use of the beryllium window increases the thickness of the cell, resulting in the need for a can with a larger stack height. A Rayovac can is used. The beryllium window fits exactly into the Rayovac can, however some sealant needs to be applied in order to prevent the electrolyte from leaking. Vacuum grease was chosen and applied in a thin layer on the remaining ring of the can surface.

Cell construction proceeded as indicated in Figure 6.1.

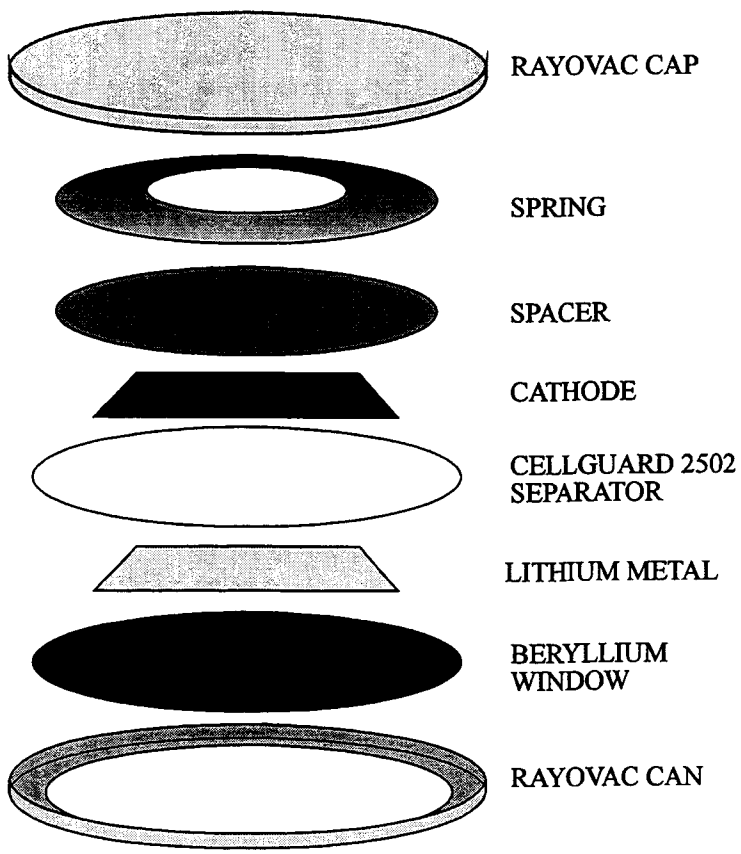

Figure 6-1: Exploded view of an in-situ cell with a lithium metal anode

A 1.2cm x 1.2cm square of lithium metal is placed above the beryllium window and then 5 to 6 drops of electrolyte are placed on the lithium metal. The electrolyte and separator are the same as those used in Section 5.2.2. The separator absorbs the electrolyte placed on the lithium metal. Above the separator is placed the electrode that contains the active material. It is placed so that the active surface is facing the beryllium window. Cell construction is completed by applying a spacer, spring and the cell cap. The cell is sealed from the environment by folding the edge of the cell can over the edge of the cap.

In this arrangement the x-rays must travel through the beryllium, lithium and the separator, all of which are covered in electrolyte, in order to reach the cathode. The result is an x-ray diffraction pattern which contains not only the desired active material peaks, but which also contains some unwanted peaks associated with the beryllium, the lithium, the separator and the electrolyte. In addition, the signal from the active material is attenuated by the absorption of x-rays by the beryllium, the lithium and the separator. Some of these undesired peaks may overlap with the active material peaks making it difficult, if not impossible, to determine their behaviour as the lithium is removed. However, with this cell design, there is no way to reverse the construction process and place the cathode next to the beryllium window, since beryllium will dissolve at voltages greater then 3V. Since most of the transition metal oxide intercalation compounds studied have voltages, versus lithium metal, of greater than 3V(see Figure 1-3) cells using lithium metal and beryllium must be constructed in the fashion described above.

6.1.3 Cell Testing

Prior to cycling, the cell must be mounted in a holder specifically designed to fit into the Phillips diffractometer. The cell is then mounted into the diffractometer. Cell testing for the in-situ cell proceeded as described in section 5.2.3. The cells were charged and discharged with constant current, and the voltage monitored until it reached a certain trip point at which time the cell current switches.

An initial scan was taken of the cell in order to get an idea of the initial peak positions. Following this, the current is programmed and cell cycling begins, as does the collection of x-ray data.

6.1.4 Results for $NaFeO_2$

The results of the preliminary scan for $NaFeO_2$ are shown in Figure 6-2, with indexed and identified peaks. Only the 101 and 110 peaks are clearly identifiable and do not overlap with other peaks. However, these peaks are fairly weak compared with separator or beryllium peaks. Should these peaks decrease in intensity due to a phase change or shift position due to changing lattice constant resulting from the removal of sodium, they could be lost in other peaks. As a result of the need to obtain an in-situ x-ray diffraction pattern that does not contain so many unwanted peaks and to get a better signal to noise ratio, an alternate in-situ technology was developed.

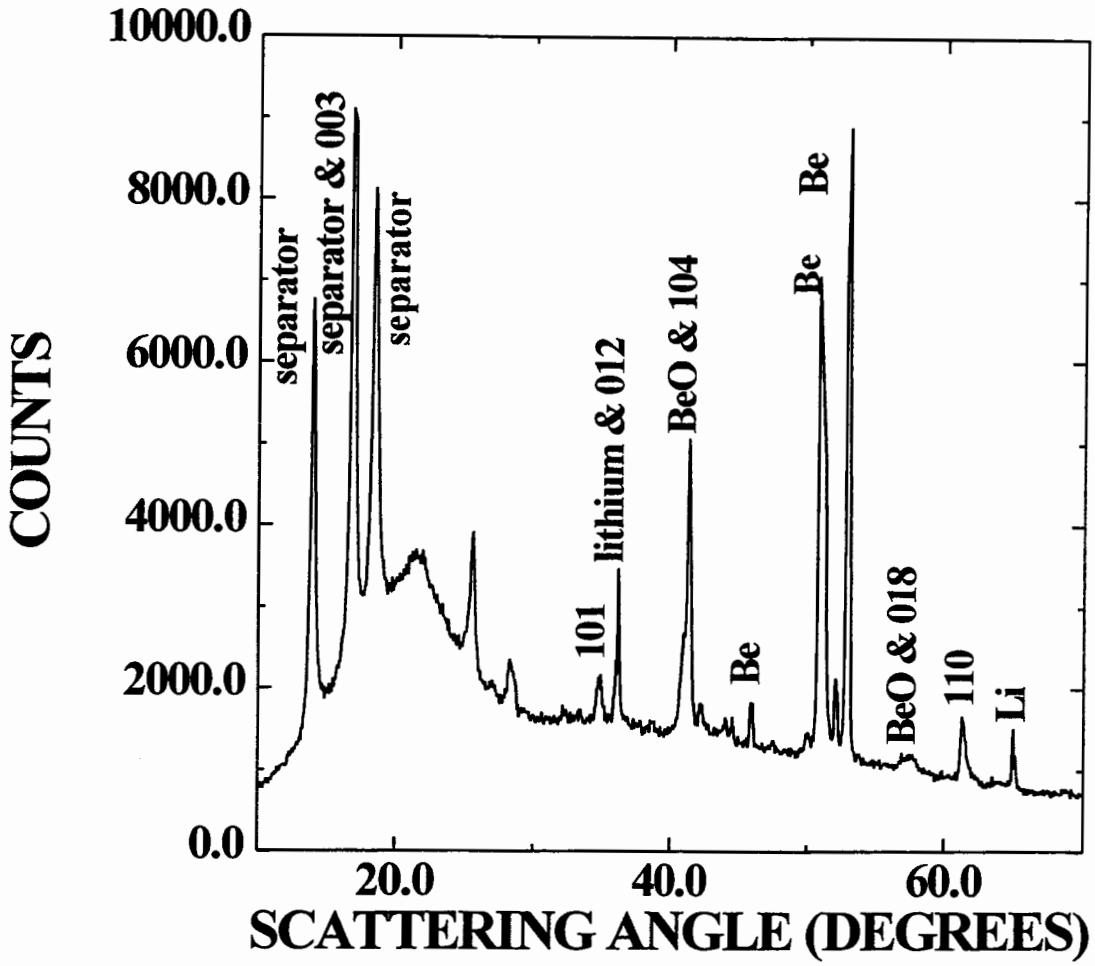

Figure 6-2: Initial x-ray diffraction pattern measured for an $NaFeO_2$ in-situ cell.

6.2 PLASTIC CELLS FOR IMPROVED IN-SITU CELLS

As mentioned in section 6.1.4, the problem with the traditional in-situ cells is the extra material the x-rays must travel through before getting to the cathode. The ideal solution would be to reverse the construction process and place the cathode next to the beryllium window. This is the idea behind the development of the Bellcore plastic electrode technology described in (Amatucci et al., 1995, Gozdz et al., 1994). In this new in-situ cell design, the electrodes contain all the electrolyte needed in the cell thereby creating a 'dry' cell.

The first step in developing this technology for the lab was to take the information in the patent (Gozdz et al., 1994) and test out the experimental procedures used to produce the electrodes. This consisted of mixing the cathode powder of choice with a solution of plasticizer and polymer, so that the electrodes come out as thin sheets of placticized material. Having accomplished this, the next step was to construct a test cell having these plastic electrodes and separator, all laminated together, and containing all the electrolyte the cell needs. The material of choice for this study was $LiMn_2O_4$ since its behaviour is well known (Xia and Yoshio, 1996). If the plastic electrodes perform well for the $LiMn_2O_4$ cell, then the studies of $NaFeO_2$ and $LiFeO_2$ can proceed.

The Bellcore technology is at this point only applicable, in an in-situ cell, if one wants to study the behaviour of a material in a lithium-ion cell, although it may at some point be possible to modify the cell construction in order to include a lithium metal anode instead of a carbon anode. For the moment, this is not the case.

6.2.1 Electrode Fabrication

Bellcore cells use 'plastic' electrodes as outlined in (Gozdz et al, 1994). The recipe varies slightly between the cathode and anode. The recipe for the cathode requires mixing:

11.1% Active material
5.6% Kynar Polymer (VdF-HFP)
1.4% Carbon Black
9.7% EC/PC
72.2% Acetone

The recipe for the anode is:

11.8% Active material

5.6% Kynar Polymer (VdF-HFP)

.70% Carbon Black

9.7% EC/PC

72.2% Acetone

where schematics for the structures of EC and PC are given in Figure 6-3

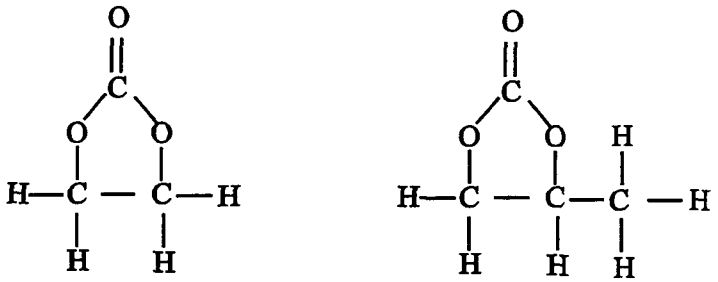

Figure 6-3: Schematic drawing of the structure of EC and PC (Zheng, 1996)

The Kynar copolymer is composed of 88% vinylidene fluoride (VdF) + 12% hexafluoro-propylene (HFP) (Gozdz et al., 1994). Schematics for the structures of each of these monomers are given in Figure 6-4

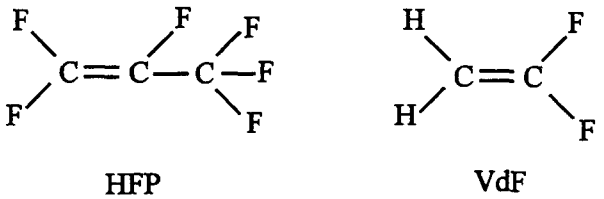

Figure 6-4: Schematic drawing of the structure of HFP and VdF monomers that compose the Kynar copolymer (Merck, 1989).

As mentioned previously, the electrolyte in the Bellcore cell is all contained in the electrodes and separator. The cathode is going next to the beryllium window, so there cannot be any excess electrolyte since it would result in the dissolution of the beryllium

window. As a result, a Celgard separator cannot be used since it requires the use of excess electrolyte in order to become sufficiently wet.

The patent (Gozdz et al., 1994) describes a variety of recipes for a separator made from the same polymer (Kynar) that is used in the electrode synthesis. In the process of developing this technology for use in the lab, several of these recipes were tested and the optimum recipe for our purposes was found to be:

1.5 g Kynar
2.0 g EC/PC
10.0 g Acetone

This recipe was found to be optimal since it has the maximum amount of EC/PC that can be added and still produce a separator with sufficient mechanical strength. The maximum amount of EC/PC is desired since most of it is later removed to produce pores into which electrolyte is absorbed. As a result, the more EC/PC present in the electrodes and separator, the more EC/PC can be removed and more electrolyte can be absorbed.

The mixtures above were placed in glass bottles, which have seals preventing the acetone from evaporating. The bottles were placed in water baths kept at a temperature of 50°C for 4 hours. The purpose of the hot water bath is to accelerate the dissolution of the Kynar polymer. A stir bar was placed in the bottle and the bottle placed on a stirrer hot plate in order to achieve a good mixture of the different constituent materials.

The mixture containing the dissolved polymer is then poured into the doctor blade spreader to produce a film. The dried film typically contains about 40% active material by weight.

6.2.2 Cell Assembly

The electrode and separator films are coated using the doctor blade. These components are ready to use as soon as the acetone has evaporated. The electrodes are cut into 1.2 x 1.2 cm squares. The separator is cut into a larger square. The cathode and separator are laminated together at 175°C using a roll laminator. Aluminum tabs are laminated onto the corners of the cathode to act as current collectors. The carbon anode is then laminated onto the other side of the separator. The entire process described above proceeds in air. The electrode 'sandwich' is soaked in ether for 5 minutes to remove EC/PC. When soaked in ether, according to (Gozdz et al., 1994), and our own trials, most of the EC/PC is removed.

The rest of the cell construction process proceeds in an argon filled glove box since electrolyte is needed. The electrode 'sandwich' is soaked in electrolyte for 5 minutes. The electrolyte, according to (Gozdz et al., 1994), moves into the pores left by the removal of the EC/PC. The sandwich is removed from the electrolyte and the excess electrolyte is blotted with a tissue.

Cell construction then proceeds as indicated in Figure 6-5. In order to prevent direct contact between the electrolyte containing cathode and the beryllium window, an aluminum spacer ring is placed next to the window. The ring is cut so that the aluminum tabs laminated onto the corners of the cathode line up with it.

Since the electrodes and separator are laminated together in this type of cell construction it is not necessary to include the spacer and spring which apply stack pressure to the components in order to ensure that the electrode contact is good. However

in order to prevent the electrodes and separator from rattling around in the cell can used, they must be included

A stainless steel spacer is placed above the carbon anode. Then a stainless steel disc spring is placed above the spacer. Finally, the cell cap is placed. The cell is then crimped so that the edge of the can folds over the cap, isolating the cell contents from the environment. The cell is now complete.

In order to proceed with the in-situ measurement, a stainless steel tab is spot welded onto the cap of the cell. The cell is then placed into a holder designed to fit into the Philips x-ray machine.

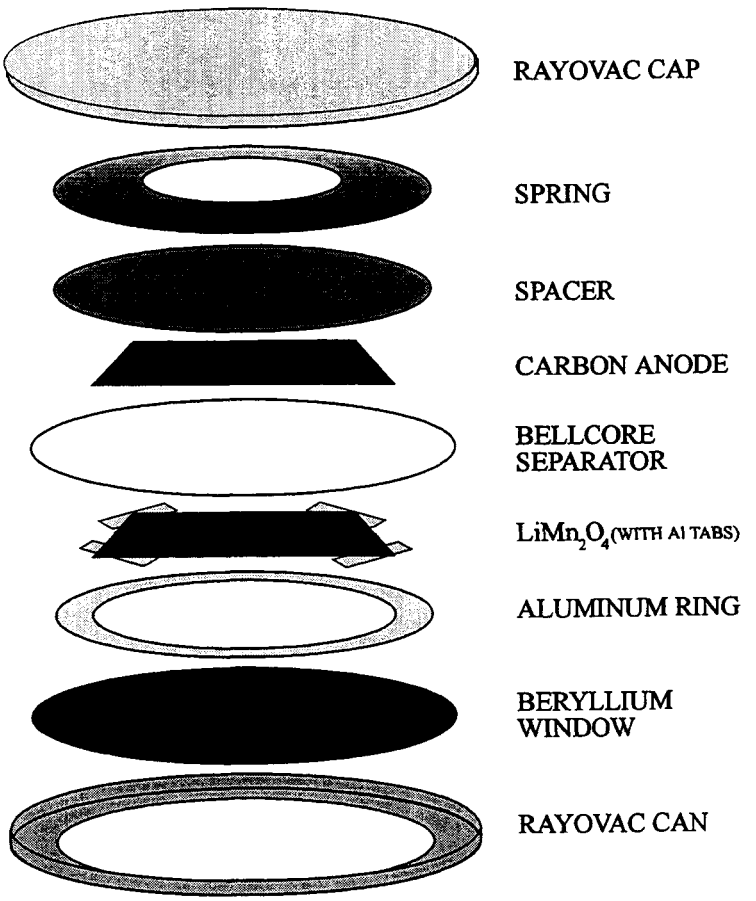

Figure 6-5: Exploded in-situ cell with plastic electrodes

6.2.3 Test of the New Cell on $LiMn_2O_4$

Although the technology was developed with the explicit purpose of being used in in-situ cells, the hardware used in the experiment by (Amatucci et al, 1995) is different from that described here. The effects of this design alteration are unknown. As a result, it was necessary to test the technology on a material whose behaviour is well known.

The manganese oxide material, $LiMn_2O_4$, was chosen for the test study. Test cells of Bellcore $LiMn_2O_4$ electrodes were made in regular cell hardware. These cells were made to ensure that the plastic technology did not affect the cycling behaviour of the $LiMn_2O_4$ material. Cell construction proceeds as shown in Figure 5-1. The plastic $LiMn_2O_4$ electrode was cut into a 1.2 x 1.2 cm square and placed at the bottom of the can. In this cell design, there is no beryllium window and as a result it is not necessary to use an aluminum ring and so it is not necessary to laminate aluminum tabs onto the corners of the cathode. Lithium metal is used as the anode and a Celgard separator was used. The lithium metal square, also cut into a 1.2 x 1.2 cm square, is placed above the separator and moved so that it was aligned with the cathode. Cell construction was completed with the addition of a stainless steel spacer and spring and the cell cap. Figure 6-6 shows the capacity of the Bellcore $LiMn_2O_4$ cell cycled versus lithium metal at a 100 hour rate.

Figure 6-6 also shows the capacity for the same $LiMn_2O_4$ powder which was used to make a cathode on an aluminum foil substrate. The method for the cathode preparations is described in section 5.2.1. The cell was cycled versus lithium metal at a 50 hour rate. Although the hour rates for these cells are different, 100 hours for the Bellcore and 50 hours for the other, the capacity and the voltage profile obtained from

the material is approximately the same for either cathode. The plastic electrode technology does not produce any adverse effect in the electrochemical behaviour of the $LiMn_2O_4$. The next step was to determine if cells constructed using the in-situ design of section 6.2.2 would have the same electrochemical behaviour and if the x-ray diffraction pattern would be cleaner than that measured in Figure 6-2. An in-situ cell was constructed following the method described in section 6.2.2 and Figure 6-5.

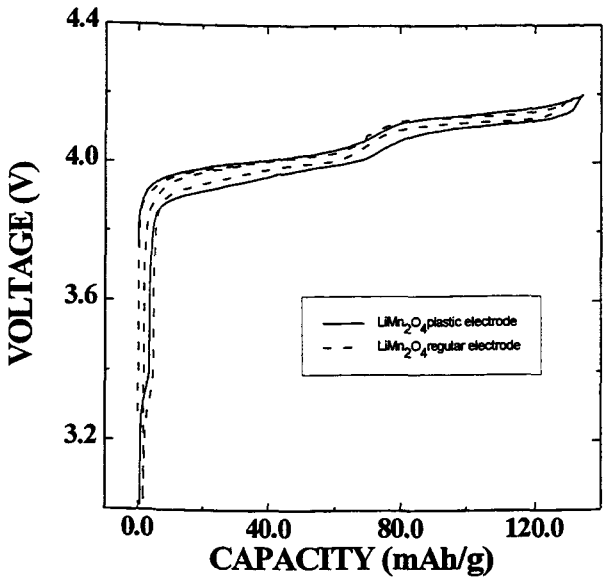

Figure 6-6: Voltage versus capacity for plastic Bellcore and regular $LiMn_2O_4$ electrodes versus lithium metal

The Miller indices and scattering angles for the $LiMn_2O_4$ peaks were obtained from CD ROM (JCPDS) and are listed in Table 7.

Table 7: The Miller indices and scattering angles and peak intensities for $LiMn_2O_4$.

h k l	Scattering Angle	Intensity (Expected)	Intensity(Measured)
1 1 1	18.785	100	95
3 1 1	36.342	90	81
2 2 2	37.933	5	not observed
4 0 0	44.141	100	100
3 3 1	48.375	10	30
5 1 1	58.355	50	38
4 4 0	64.177	90	53
5 3 1	67.306	30	25

Figure 6-7 shows the preliminary diffraction data taken for a fresh $LiMn_2O_4$ in-situ cell. There are no separator or lithium peaks in this measured data for the $LiMn_2O_4$ in-situ cell. As a result many more of the peaks from the active material are visible and none overlap with the BeO or Al peaks. The signal-to-noise ratio of the data is also much better than that measured for $NaFeO_2$ in Figure 6-2. The aluminum peaks are due to reflections from the aluminum ring and the aluminum tabs laminated onto the cathode. There is still a broad peak visible at approximately 20^0, which is due to the polymer present in the plastic cathode and in the separator pieces used to laminate the aluminum tabs onto the cathode.

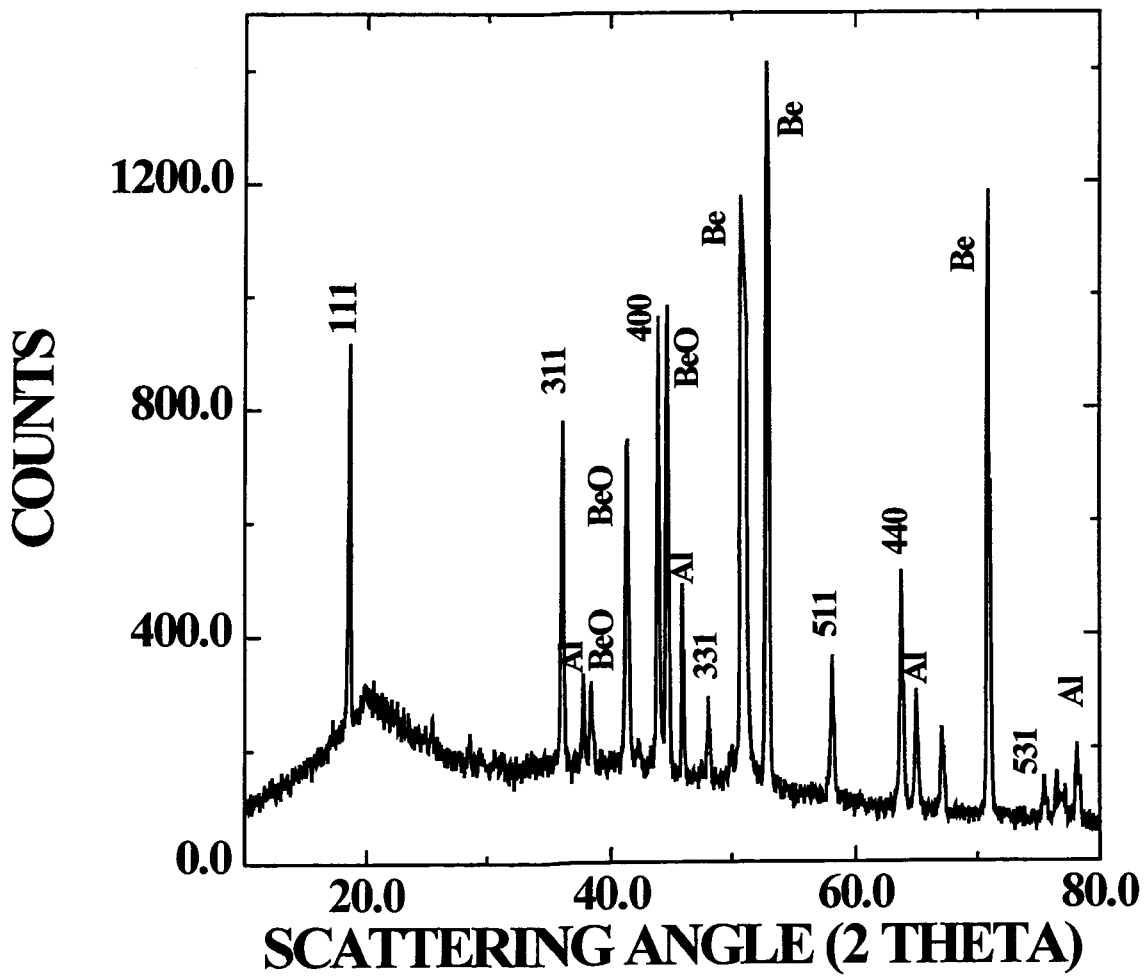

Figure 6-7: Initial x-ray diffraction pattern measured for a fresh $LiMn_2O_4$ in-situ cell

The in-situ cell using the plastic electrodes are cycled versus a carbon anode. As a result, the voltage profile is different from when the anode is lithium metal because carbon has the ability to intercalate lithium and has a voltage versus lithium which varies with x in Li_xC_6 . The voltage profile for a carbon versus lithium anode cell constructed as in Fig 5-1 is shown in Figure 6-8. The voltage profile for an $LiMn_2O_4$ cell versus lithium metal is also shown in Figure 6-8. Theoretically, the expected voltage profile for a cell having $LiMn_2O_4$ versus carbon can be calculated by subtracting the carbon profile from the $LiMn_2O_4$ profile. This was done and the result is the dashed line in Figure 6-8. The actual measured voltage profile is the solid line in Figure 6-8.

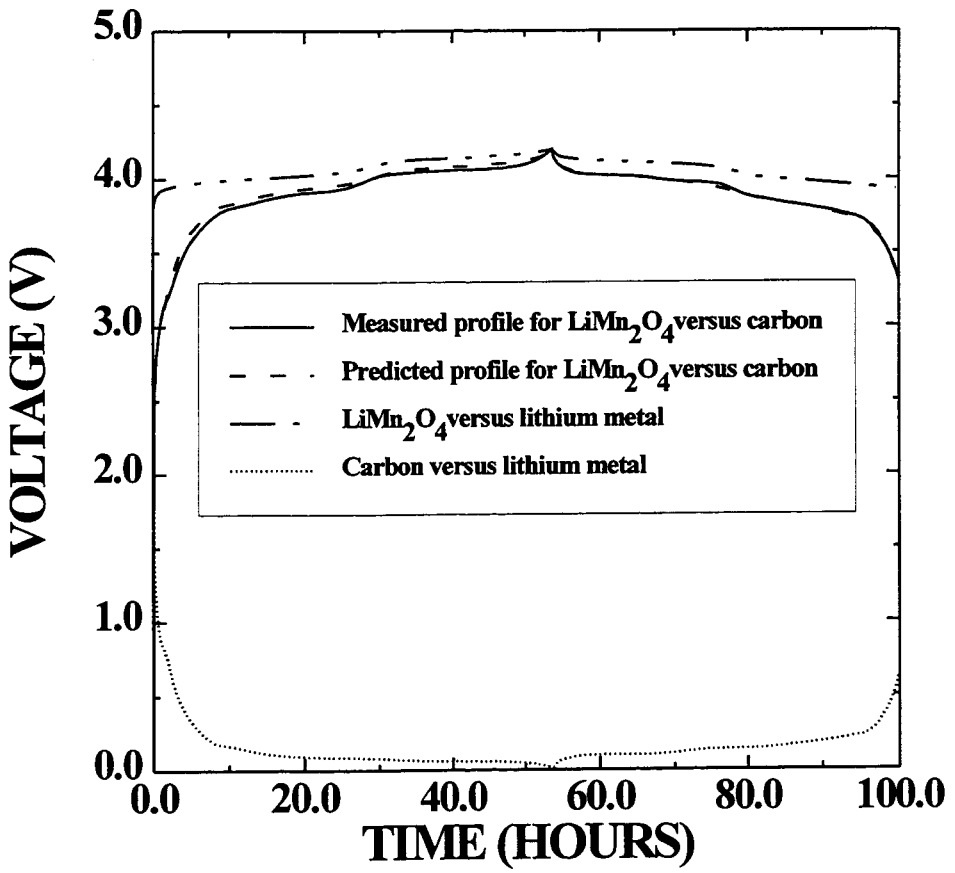

Figure 6-8: Measured voltage profiles for carbon and $LiMn_2O_4$ versus lithium metal and the predicted and measured voltage profiles for $LiMn_2O_4$ versus carbon

The voltage profile shows that the theoretical voltage profile is the same as the measured voltage profile. The question remains however, what do the x-ray diffraction data look like?

This cell was cycled at a 50 hour rate for 2 cycles. The voltage profile is shown in Figure 6-9. It is the same profile as shown in Figure 6-8 above.

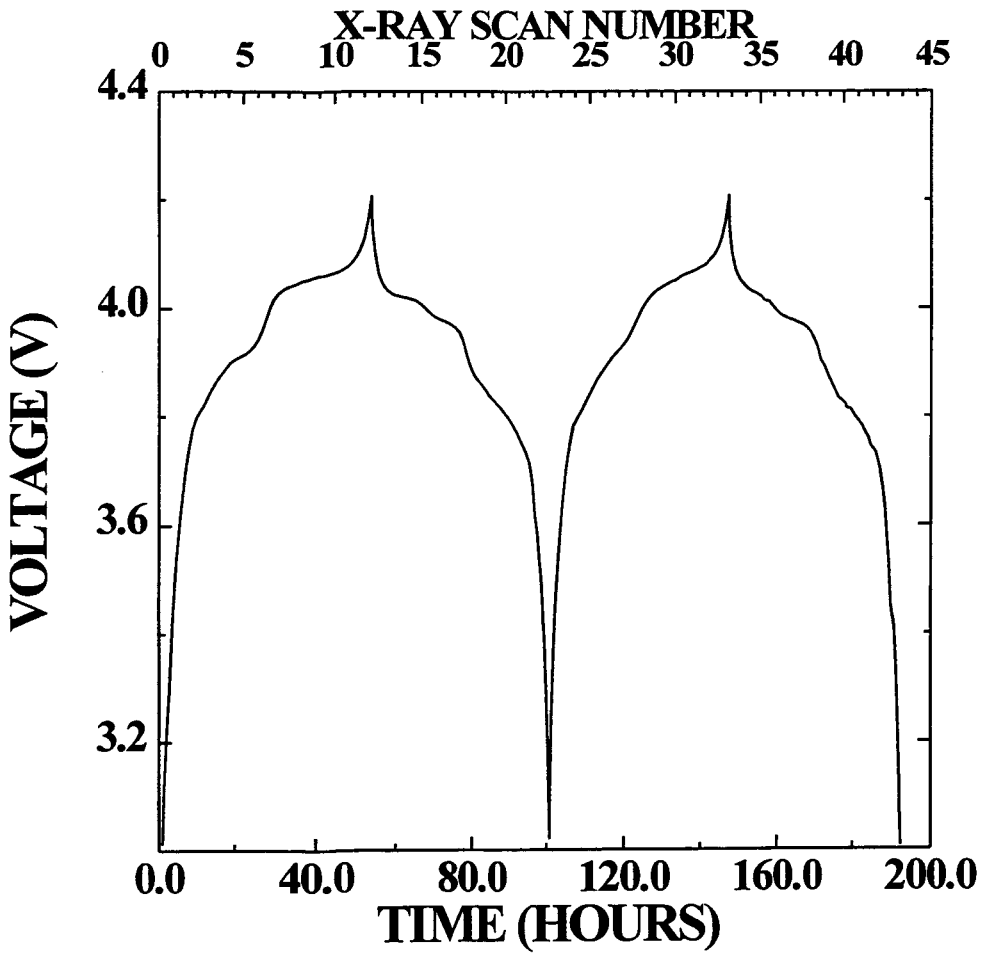

Figure 6-9: Voltage profile for the Bellcore $LiMn_2O_4$ in-situ cell with scan number indicating the 37.5° termination point

While the cell was being cycled, one of the ranges the x-ray detector repeatedly scanned was from 35 to 37.5° so that the displacement of the initial 311 peak and the development of the two phase region could be observed. The scan number in Figure

6-9 shown the times at which the scattering angle reached its terminal value of 37.5°. The first discharge is slightly shorter than the first charge, due to the irreversible capacity occurring as a result of the reaction between the electrolyte and the carbon surface.

If the 311 peak is examined it is possible to obtain some information concerning the behaviour of $LiMn_2O_4$ as lithium is removed. Figure 6-10 shows the 311 peak during the first charge as lithium is removed.

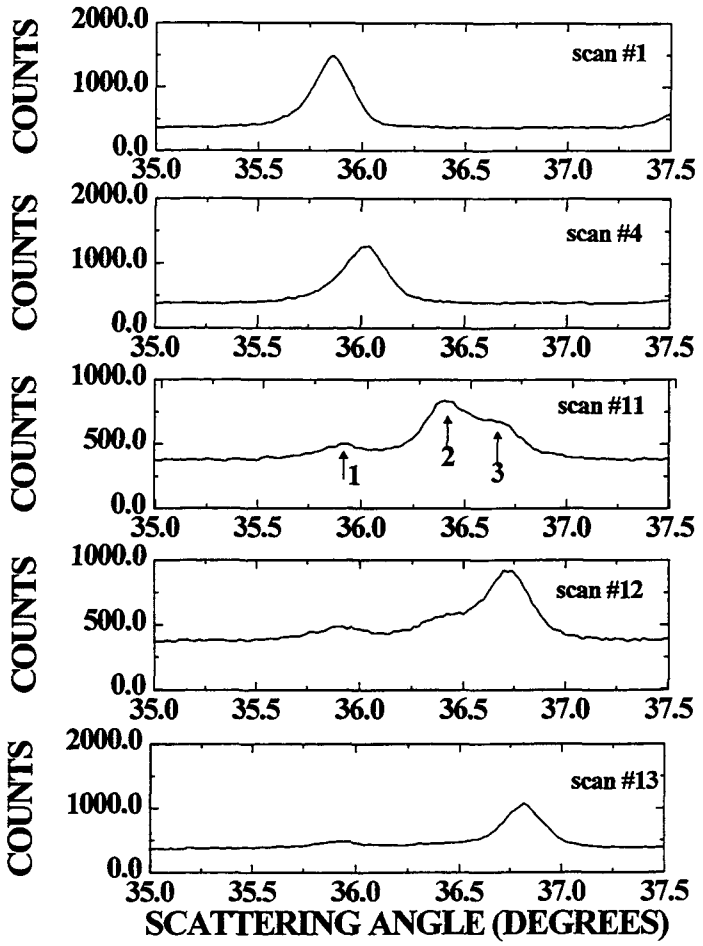

Figure 6-10: Shows the shift in the position of the 311 peak as lithium is removed from the $LiMn_2O_4$.

Initially the peak shifts to the right, corresponding to an increasing scattering angle or a decreasing d-spacing due to the removal of lithium. At scan # 11, there are clearly two

peaks present at approximately 36.5° and another peak at approximately 36°. The latter peak is attributed to some small amount of disconnected grains which are not available to de-intercalate lithium. The two peaks at approximately 36.5° correspond to two coexisting phases of lithium manganese oxide. As more lithium is removed, the intensity of the 2nd phase grows, thereby confirming that the second peak in #11 belongs to a phase of $Li_{(1-x)}Mn_2O_4$ that has had more lithium removed from it. Eventually, all the lithium that can be removed has been removed and the peak corresponding to the phase with the least amount of lithium present is dominant.

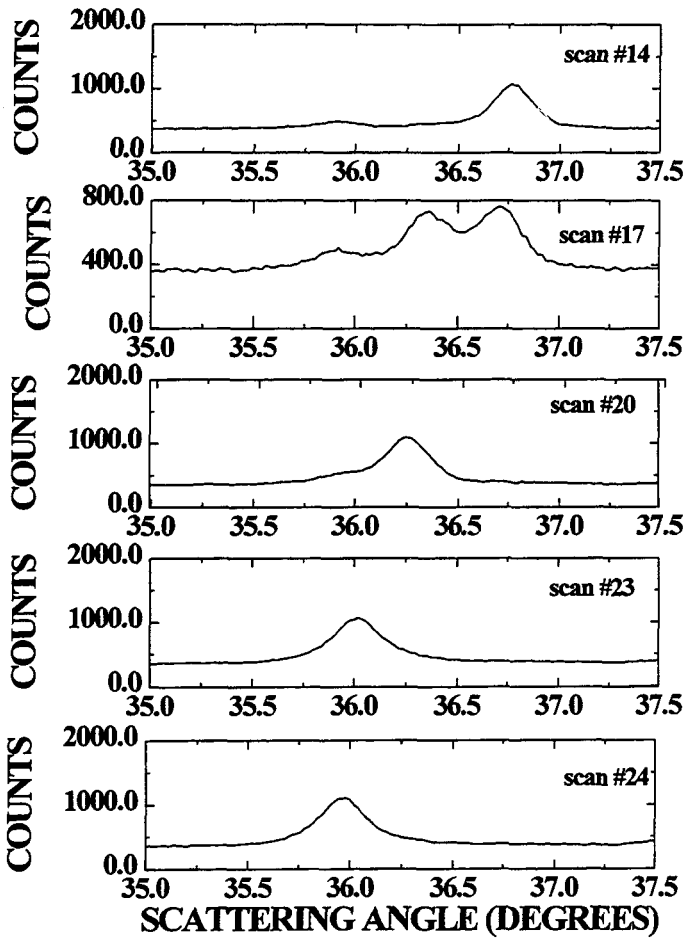

Figure 6-11: Shows the shift in the 311 peak as lithium is re-inserted into $LiMn_2O_4$ on discharge.

Figure 6-11 shows the 311 peak observed during the first discharge. We saw from the voltage profile, Figure 6-9, that the removal of lithium is reversible. The re-insertion of the lithium into the lattice is observed in the x-ray diffraction pattern by the shift of the 311 peak to the left of its position when discharge started.

Figure 6-12 shows the scattering angle of the 311 peaks plotted versus x in $Li_{1-x}Mn_2O_4$. The amount of lithium removed, x, from the cathode material is calculated by multiplying the known current by the time and dividing by the active mass. This calculates the capacity for that particular time. Theoretically, if all the lithium were removed from the material, x=1, the specific capacity given by equation 5-8 would be 148mAh/g. By calculating the ratio of the calculated capacity to the specific capacity, the value of x can be determined.

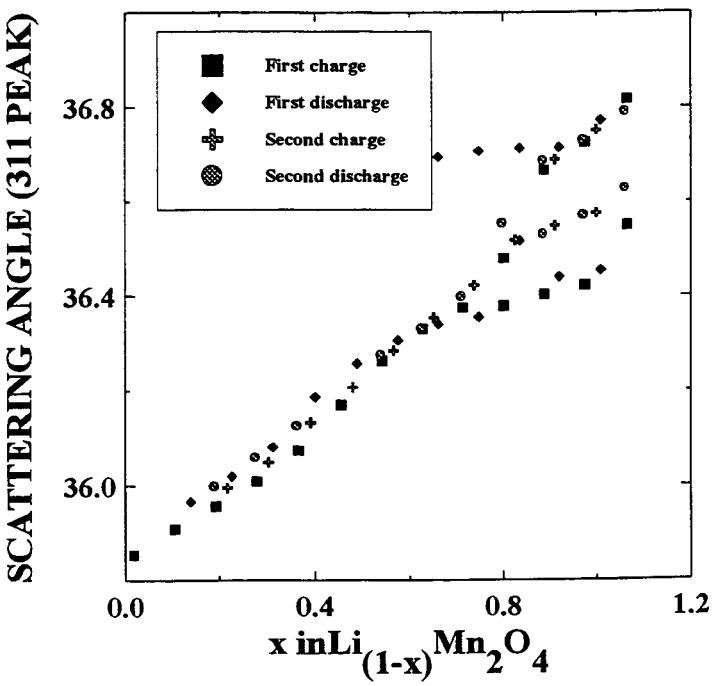

Figure 6-12: The position of the 311 peak versus lithium content x

In order to be sure that the plastic electrode technology has no adverse effects on the electrochemical behaviour of $LiMn_2O_4$, the lattice constants, a, were calculated from the 311 peak positions. The calculated lattice constants are plotted versus x in Figure 6-13.

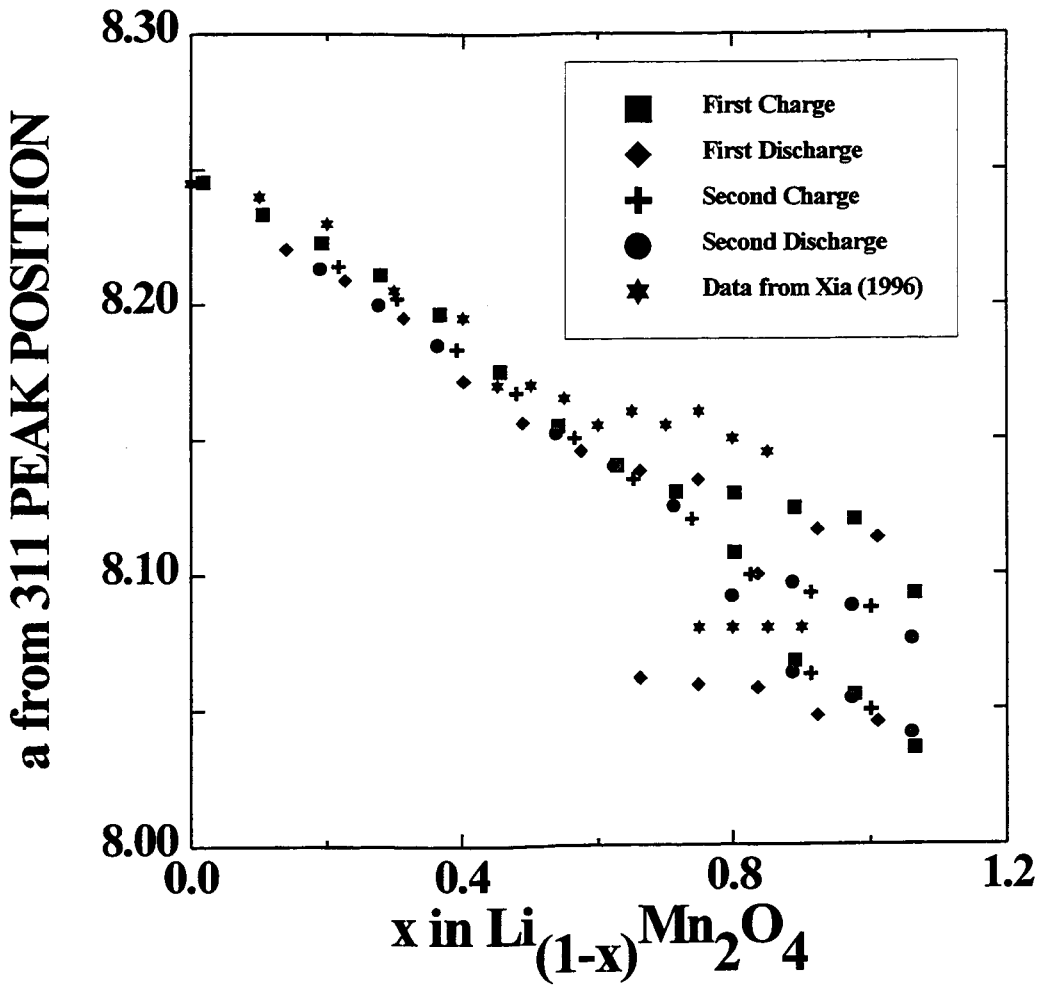

Figure 6-13: Lattice constant versus x for the $LiMn_2O_4$ in-situ cell.

Since the lattice constants were calculated from single peaks, there are no error estimates. If Figure 6-13 is compared with data measured by Xia et al. (1996) it is found that both exhibit a decrease in the lattice constant as lithium is removed until the point

when the 2 phase region forms. The lattice constant of the initial materials agree well, as do the lattice constants up to about x=0.6. The lattice constants for the two phase region are slightly different. In the data measured by Xia and Yoshio (1996), they observed a lattice constant of 8.16 for the upper plateau and 8.08 for the lower plateau. The data we measured has a lattice constant of 8.13 for the upper plateau and 8.06 for the lower plateau. The reason for the difference is unclear. Perhaps this difference could be attributed to different compound stoichiometries. It is known what the stoichiometry of the material used in this study is $Li_{1.02}Mn_{3.98}O_4$.

Based on data above, which clearly shows the same features observed by Xia and Yoshio. (1996) it can be concluded that the plastic electrode in situ cell technology appears to work well on $LiMn_2O_4$. The next step is to try the technology on $NaFeO_2$ and $LiFeO_2$.

6.3 Result of In-Situ Measurements on $NaFeO_2$ and $LiFeO_2$

6.3.1 $NaFeO_2$

An $NaFeO_2$ plastic electrode was made according to the cathode recipe outlined in section 6.2.1. The cathode is cut into 1.2 x 1.2 cm squares. Cell construction proceeds as described in section 6.2.2.

The initial x-ray scan for the $NaFeO_2$ material is given in Figure 6-14.

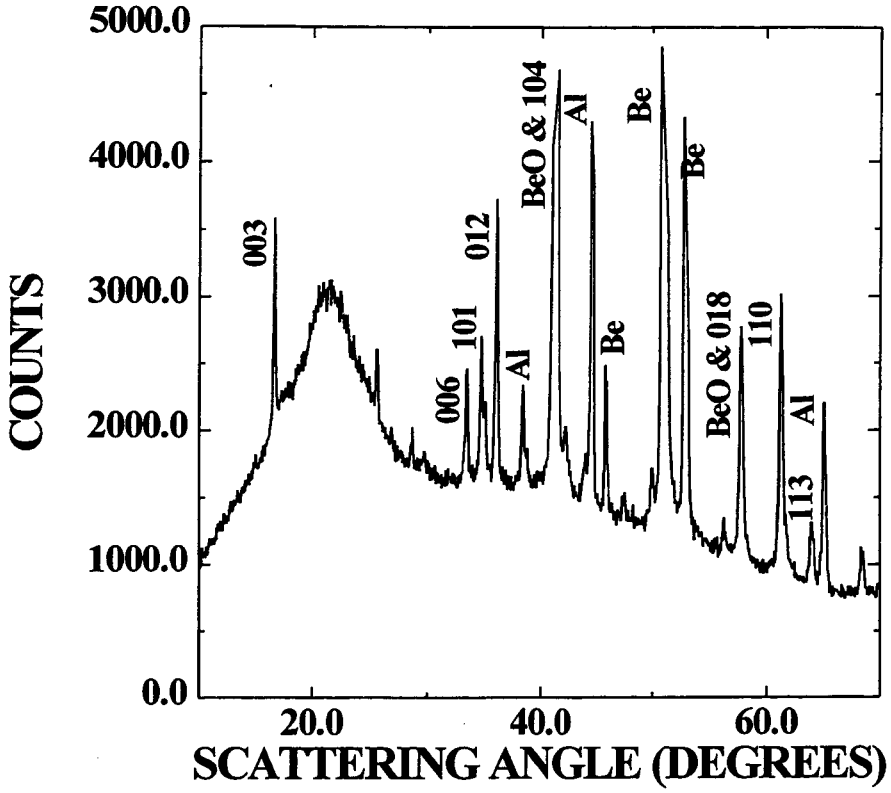

Figure 6-14: Initial x-ray diffraction data measured for a fresh $NaFeO_2$ in-situ cell

Compared with Figure 6.2, which was the initial scan for the old in-situ cell design, this scan is much cleaner and the signal to background is much better. Most of the peaks do not overlap with any others.

The plastic electrode technology appears to work well with the $NaFeO_2$ material. The voltage profile of the material, versus carbon, is shown in Figure 6-15. The cell was cycled at a 100 hour rate to 4.7V. Since the cell was cycled versus carbon, the voltage profile is different from the one shown in Figure 5-3. The reason for this difference is the same as for $LiMn_2O_4$ given on page 65.

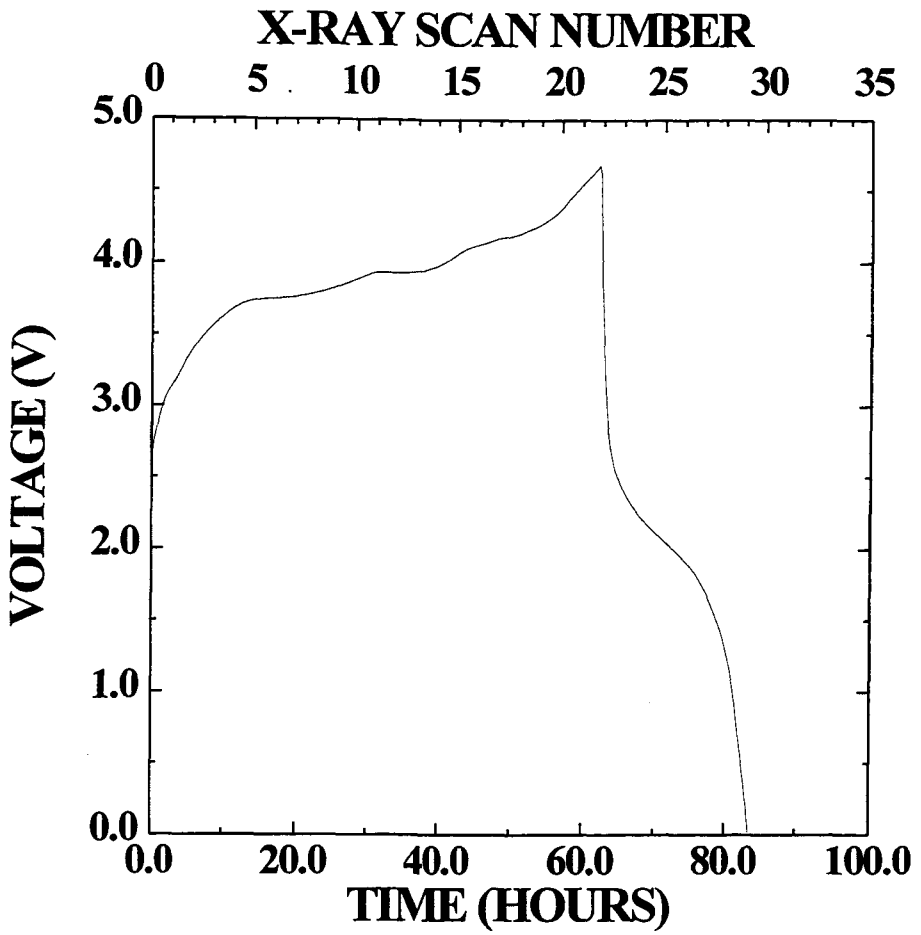

Figure 6-15: Voltage profile for Bellcore plastic $NaFeO_2$ versus carbon in-situ cell

As opposed to the cells studied versus lithium metal, this in-situ cell was discharged to 0.0V. Below 3.0V, there is a plateau, which was not observed before because the cells were not discharged below 3.0V. It is much shorter than the one observed on charge, so the mystery of what occurs on charge still remains. The mystery centers on two phenomena which should be occurring in the cell. The first is the removal of sodium atoms from the iron oxide lattice on charge, which is indicated by the plateau from 3.7 to 4.7V. Ideally, the removal of the sodium atoms from the cathode should be followed by the insertion of sodium atoms into the carbon. However, it is well known that sodium atoms do not intercalate appreciably into graphitic carbons like our anode material (Di

and Mele, 1985). If the sodium does not enter the carbon, then it must remain in the electrolyte. Let's say that 60% of the sodium is removed from the iron oxide lattice on charge. Then if the mass of the active material in the cathode is 20mg, the number of moles of sodium that enter the electrolyte can be determined from:

$$\frac{M_a}{W_m} * 60\% \qquad (6\text{-}1)$$

where M_a is the mass of active material and W_m is the molecular weight. For an active mass of 20mg there would be 0.00011 moles of sodium atoms in the electrolyte following a charge where 60% of the sodium atoms were removed. Assuming that 0.2mL of electrolyte was used during cell construction, then there are 0.0002 moles of $LiPF_6$ salt and so 0.0002 moles of lithium ions in the electrolyte. After charge the electrolyte could contain up to 67% sodium atoms, whose effects on the electrolyte conductivity are unknown.

Figure 6-16 shows a section of the x-ray diffraction data measured as the cell was cycled. As was the case for $LiMn_2O_4$, x-ray data collection focused on certain peaks in the profile so that good statistics were obtained for those regions.

The peaks broaden as the sodium is removed. As mentioned previously, x-ray data was only collected in specific regions where $NaFeO_2$ reflections occurred. As a result, if a new phase was formed resulting in peaks in a new region, these would not have been observed. On discharge, the peaks sharpen up again, however the position of the peaks has changed. Specifically, the 110 peak shifts from an initial angle of 61.353°

to 61.517° at scan #31. The broadened peaks on charge would indicate that sodium is removed from the material because they indicate a change in the bulk structure of the host. The broadening may indicate that the distance between layers is no longer definite. The sharpening of the peaks on discharge indicates that during the plateau at 3.0V some atoms do re-enter the structure. Whether these atoms are lithium or sodium is unknown, since both are in the electrolyte.

Since the in-situ cell finished at night, extra data was collected when the cell was not being cycled. The last scan measured was # 35. It shows that the lattice is still intact after cycling is complete.

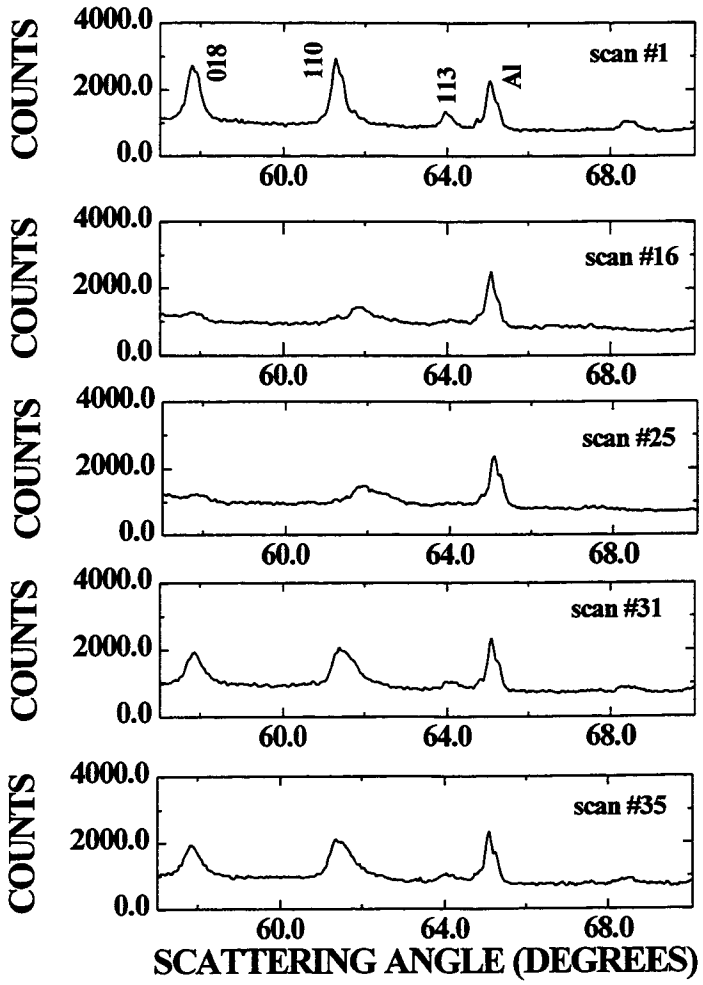

Figure 6-16: X-ray diffraction data measured as the $NaFeO_2$ in-situ cell was cycled.

The in-situ measurement shows that sodium atoms can be reversibly de-intercalated to some extent, however the process is not totally reversible. Of course, the material of greatest interest is $LiFeO_2$.

6.3.2 $LiFeO_2$

The $LiFeO_2$ plastic electrode was made according to the recipe described in section 6.2.1. The cell was built as described in section 6.2.2.

The preliminary x-ray scan for the $LiFeO_2$ cell is shown in Figure 6-17. As was the case for $NaFeO_2$, the peaks are clearly identifiable.

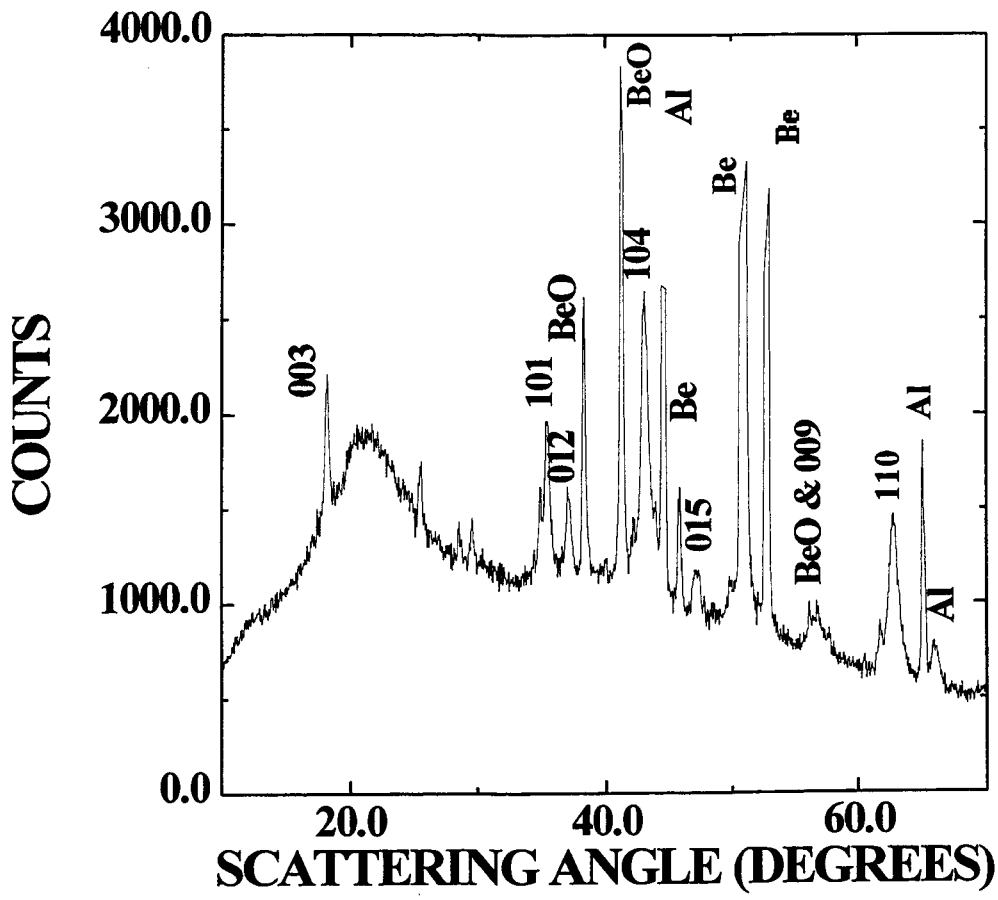

Figure 6-17: Initial x-ray data measured for the plastic $LiFeO_2$ versus carbon in-situ cell.

The cell was cycled at a 100 hour rate. The voltage profile for the cell is shown in Figure 6-18. At one point, cell cycling was stopped for maintenance, leading to a slight amount of self discharge. However, the voltage quickly returned to its original value once cycling restarted.

The cell was cycled to 5.3V in the first cycle, which is a voltage significantly higher than the 4.7V cutoff used for the data shown in Figure 5-3. The high voltage results in a very large, very flat plateau, from approximaterly 5.1V to 5.2V, which had not been observed previously. The discharge was very similar to that seen in Figure 5-3, indicating that if lithium is removed from the material during this charge, it is not returned to the material during discharge, even when the cell is discharged to 1.0V as seen in Figure 6-18.

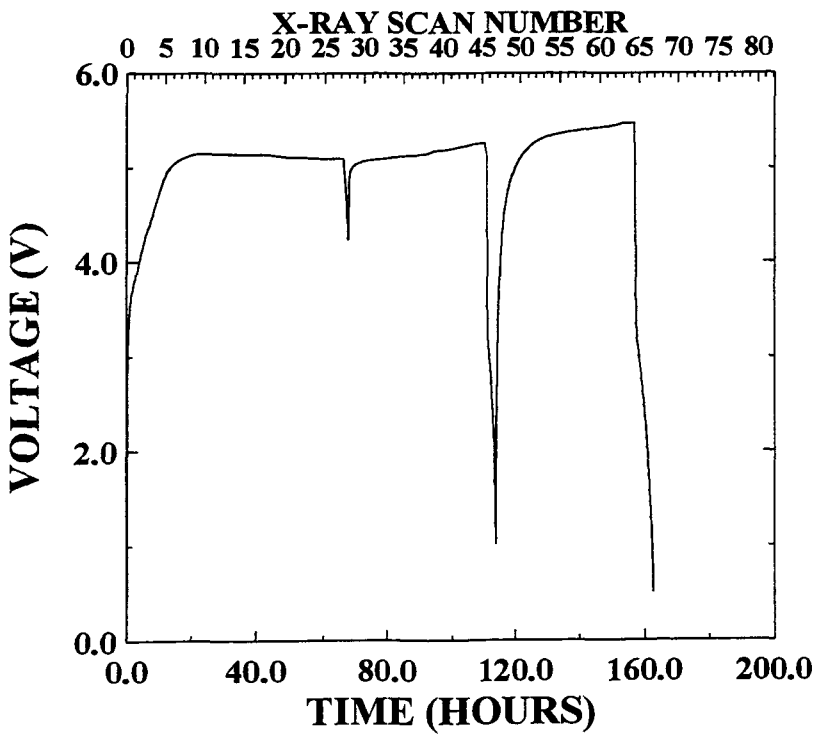

Figure 6-18: Voltage profile for the Bellcore $LiFeO_2$ in-situ cell

The question remains, is lithium removed during the flat plateau on charge? The in-situ x-ray diffraction pattern obtained halfway through the plateau and at the end of the charge are shown in Figure 6-19 and compared with the initial scan. The patterns are offset by 1000 counts in order to make it easy to see differences between the patterns.

There are no new peaks and no changes in peak intensity. As a result, one can only conclude that lithium is not removed from the material The cause of the plateau visible on charge in Figure 6-18 is then from a different mechanism. Somehow, there is a significant amount of charge being transferred from the cathode to the anode. If the cathode material is not the source then there are only two other possibilities. The first is electrolyte decomposition and the second is that the beryllium window could be dissolving if the cathode somehow contacted it.

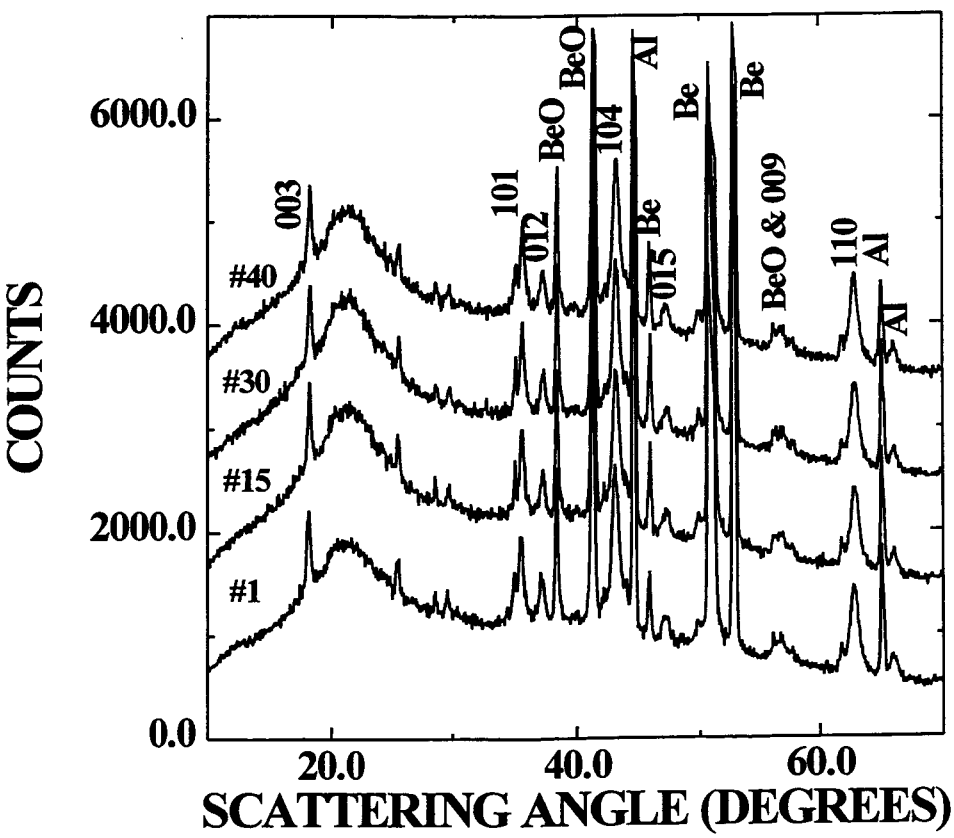

Figure 6-19: X-ray diffraction data measured for the $LiFeO_2$ plastic electrode in-situ cell

Cyclic voltammetry techniques were used by Dr. Zhang in Dr. Dahn's lab in order to determine if the electrolyte decomposes at voltages in excess of 5V. The technique involves constructing a cell in regular cell hardware. The electrodes in this cell are a lithium metal anode and a square of aluminum foil. This combination of electrodes means the cell has no capacity. The electrolyte of choice is used in order to wet the separator.

There are two electrolytes which are commonly used in the lab for electrochemical studies. They are

1) 1M $LiBF_4$ in a (70/30)(v/v) mixture of EC/DEC

2) 1M $LiPF_6$ also in a (70/30) (v/v) mixture of EC/DEC

The later electrolyte is the one used throughout this study.

A potentiostat is then used to sweep the voltage of the cell up at a constant rate. The current is measured as the voltage increases. The results of the cyclic voltammetry study are shown in Figure 6-20.

The dashed curve is the data obtained for the cell containing the $LiBF_4$ electrolyte. In this cell, a small current starts flowing at 4.0V. Since there are no other current sources in the cell, the electrolyte must be decomposing. As for the cell containing the $LiPF_6$ electrolyte, it also indicates that there is some small current flow above 3V and this flow increases to a maximum at approximately 5V.

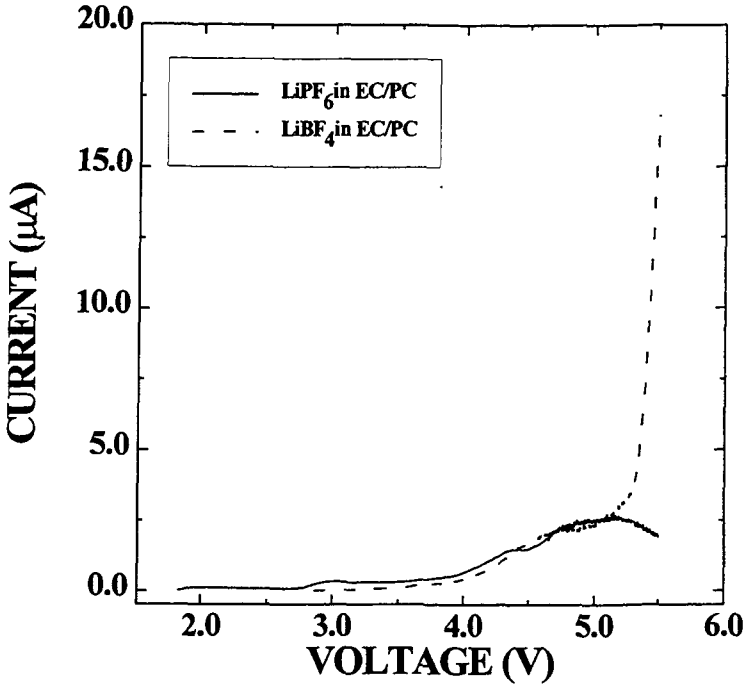

Figure 6-20: Cyclic voltammetry results for the $LiBF_4$ and $LiPF_6$ electrolytes.

Given this data, it seems pretty conclusive that the behaviour of the $LiFeO_2$ cell shown in Figure 6-18 is caused by the decomposition of the $LiPF_6$ electrolyte.

Concerning the possibility of beryllium dissolution, the beryllium window was examined once the cell was opened in order to determine if any visible damage had been done. No damage was visible. Given the amount of charge transferred to obtain the plateau in Figure 6-18, there should have been some visible damage to the window if the current transferred was due to beryllium dissolution.

Based on these two pieces of information, the only conclusion that can be drawn is that the long, flat plateau observed at 5.0V in the $LiFeO_2$ in-situ cell is caused by electrolyte decomposition.

CHAPTER SEVEN

7. CONCLUSIONS

$LiFeO_2$ and $NaFeO_2$ were synthesized and studied structurally and electrochemically. In order to do the structural work properly, it was necessary to design and implement a new in-situ x-ray cell which used 'plastic' electrodes. These new plastic electrodes and the new in-situ cell design were shown to work well on test experiments done on $LiMn_2O_4$.

We've shown that electrochemical methods cannot be used to completely replace sodium atoms in the layered sodium iron oxide material, with lithium atoms present in the electrolyte. Electrochemical studies showed that some sodium can be removed from $NaFeO_2$ on charge. On discharge, only a small portion of the atoms removed on charge can be re-inserted. In-situ x-ray diffraction data indicate that the layered structure of the iron oxide material is not destroyed by the removal of the sodium atoms so the inability to insert atoms into the lattice on discharge is not caused by a phase change.

This knowledge, combined with information that sodium atoms do not intercalate into graphitic carbons, led to the conclusion that the sodium atoms removed on charge were present , in large concentration, in the electrolyte. The presence of the sodium atoms in the electrolyte has an unknown effect on the conductivity of the electrolyte.

The electrochemical behaviour of the layered $LiFeO_2$ material was also examined. The cells used were charged to 4.7V. The voltage profiles for the cells showed that at most 7% of the lithium contained in the material could be removed. Since this material has the same structure as $LiNiO_2$ and $LiCoO_2$, which are known to reversibly intercalate

lithium, the removal of such a small amount of lithium is surprising. In order to find out why so little lithium was removed, an in-situ cell was cycled to 5.3V. The resulting voltage profile showed a very long, very flat plateau at approximately 5.2V. The x-ray data collected during charge showed no peak shift which would correspond to lithium removal from the $LiFeO_2$. This information, combined with cyclic voltammetry data concerning the decomposition of the electrolyte led to the conclusion that lithium was not removed from the $LiFeO_2$.

The objective of the thesis was to determine if lithium could be removed from the layered $LiFeO_2$ material. This question has been partially answered. Using state of the art electrolytes, it was found that lithium could not be removed. However, the voltage limit of the electrolyte was approximately 5V. So in fact in this study we've determined that lithium cannot be removed from the layered $LiFeO_2$ material below a voltage of 5V. This is not proof that lithium cannot be removed from the structure.

SUGGESTIONS FOR FURTHER WORK

Since it was found that sodium could be removed from the layered $NaFeO_2$ lattice, it is probably worthwhile to examine the electrochemical behaviour of $NaFeO_2$ versus sodium metal in order to determine if sodium can be reversibly intercalated into the iron oxide lattice. This may have implications for sodium-ion cells.

For $LiFeO_2$, we've shown that given the electrolytes currently available, which decompose above 5V, lithium cannot be removed. However, if an electrolyte stable

above 5V should become available, the electrochemical behaviour of the layered $LiFeO_2$ should be re-examined.

However, for the moment, material development should focus on more promising materials that are compatible with the existing electrolytes. These materials are $LiNiO_2$, $LiCoO_2$, $LiMn_2O_4$ and $LiMnO_2$.

REFERENCES

1) Amatucci, G.G., Tarascon, and J.M., Klein, L.C, J. Electrochem. Soc., V143, 1114 (1996).

2) Anderson, J.C., Schieber, M., J. Phys. Chem. Solids, V25, pp. 961-968 (1964).

3) Brunel, M., de Bergevin, F., J. Phys. Chem. Solids, V30, pp. 2011-2021 (1969).

4) Brunel, M., de Bergevin, F., J. Phys. Chem. Solids, V29, pp. 163-169 (1968).

5) Cox, D.E., Shirane, G., Flinn, P.A., Ruby, S.L., and Takei, W.J., Phys. Rev., V132(4), pp.1547-1553, (1963)

6) Cullity, B.D., Elements of X-Ray Diffraction, 2nd edition, Addison-Wesley, (1978).

7) Dahn, J.R., McKinnon, W.R., Physics in Canada, pp. 93-99, July (1988).

8) Dahn, J.R., von Sacken, U., Juzkow, M.W., and Al-Janaby, H., J. Electrochem. Soc., V138(8), pp. 2207-2211, (1991).

9) Di Vincenzo, D.P., Mele, E.J., Phys. Rev. B, V32 (4), pp 2538, (1985).

10) Famery, R., Bassoul, P, and Queyroux, F, J. Solid State Chemistry, V57, pp. 178-190, (1985).

11) Gozdz, A.S., Schmutz, C.N., Tarascon, J.M., and Warren, A.C., Patent Cooperative Treaty Application, PCT/US94/08772, August, 1994.

12) Hewston, T.A., Chamberland, B.L., J. Phys. Chem. Solids, V48(2), pp. 97-108, (1987).

13) Hill, R.J., Howard, C.J., J. Appl. Crystallography, V18, 173, 1985.

14) International Tables for X-Ray Crystallography, Volume1, Symmetry Groups, Kynoch Press, Birmingham England, 1969.

15) JCPDS - International Centre for Diffraction Data, Version 2.14 PDF-2 Database, Copyright (c) 1987-1993 JCPDS-ICDD, Newton Square, PA, 19073, USA.

16) Kikkawa, S, Ohkura, H., and Koizumi, M., Materials Chemistry and Physics, V18, pp. 375-380, (1987).

17) Nalbandyan, V.B., Shukaev, I.L, Russian Journal of Inorganic Chemistry (translated from Zhurnal Neorganicheskoi Khimii V37, pp. 808-810, 1987), V32(3), pp. 453-453, (1987).

18) Reimers, J.N, Fuller, E.W., Rossen, E., and Dahn, J.R., J. Electrochem. Soc., V140(12), pp. 3396-3401, December (1993).

19) Reimers, J.N., Dahn, J.R., J. Electrochem. Soc. V139(8), pp. 2091-2097, August (1992).

20) Takeda, Y., Akagi, J., Edagawa, A., Inagaki, M., and Naka, S., Mat. Res. Bull, V15, pp. 1167-1172, (1980).

21) The Merck Index, Centennial Edition, Merck & Co., (1989).

22) Way, B, Ph.D Thesis, Simon Fraser University, September 1995.

23) Xia, Y., Yoshio, M., J. Electrochem. Soc., V143(3), pp. 825-833, March 1996.

24) Zheng, T, Ph.D. Thesis, Simon Fraser University, May 1996.